

# Telegrapher’s Generative Model via Kac Flows

Richard Duong\*    Jannis Chemseddine\*    Peter K. Friz    Gabriele Steidl

October 29, 2025

## Abstract

We break the mold in flow-based generative modeling by proposing a new model based on the damped wave equation, also known as telegrapher’s equation. Similar to the diffusion equation and Brownian motion, there is a Feynman-Kac type relation between the telegrapher’s equation and the stochastic Kac process in 1D. The Kac flow evolves stepwise linearly in time, so that the probability flow is Lipschitz continuous in the Wasserstein distance and, in contrast to diffusion flows, the norm of the velocity is globally bounded. Furthermore, the Kac model has the diffusion model as its asymptotic limit. We extend these considerations to a multi-dimensional stochastic process which consists of independent 1D Kac processes in each spatial component. We show that this process gives rise to an absolutely continuous curve in the Wasserstein space and compute the conditional velocity field starting in a Dirac point analytically. Using the framework of flow matching, we train a neural network that approximates the velocity field and use it for sample generation. Our numerical experiments demonstrate the scalability of our approach, and show its advantages over diffusion models.

## 1 Introduction

Among generative neural models, flow-based techniques as score-based diffusion and flow matching stand out for their simple applicability and good scaling properties. The general idea is to construct a probability flow which starts in a simple latent distribution and leads to a possibly complicated target distribution. A neural network is then trained to learn this flow while using only a few samples from the target. In *score-based diffusion models* [35, 36], the so-called score is learned which directs the drift-diffusion flow backwards in time from the latent to the target via a certain reverse SDE. In *flow matching* [19, 20, 21] the velocity field is learned enabling the calculation of the flow’s trajectories via a certain flow ODE. These two approaches produce state-of-the-art results not only in pure sample generation, but can also be incorporated into inverse problem solvers, see e.g. [24, 46]. A unifying perspective can be given via the “stochastic interpolants” framework, see [1, 2].

Very few research has dedicated itself to explore new ways of flow modeling using other physics-inspired PDEs. In [44], a physics-inspired generative model was proposed using the Poisson equation. The authors of [22] pointed to further *physical processes and PDEs* and generally examined them with respect to their applicability in generative modeling, among them approaches based on the Schrödinger equation, Helmholtz equation, and the above-mentioned Poisson and diffusion equation. More generally, they identify two conditions mandatory for a model to be suited for data generation:

---

<sup>0</sup>Institute of Mathematics, TU Berlin, Straße des 17. Juni 136, 10623 Berlin, Germany, {duong, chemseddine, friz, steidl}@math.tu-berlin.de

\*With equal contributions. Corresponding authors.

1. "Well-behaved density flow": Initial probability densities stay probability densities, and their evolution is well-behaved.
2. "Asymptotic behavior": Long-term convergence of the flow to a (known) stationary distribution independent of the initial distribution.

The first condition can be split into two separable conditions: *conservation of mass* and *regularity of the flow*. While the meaning of the former is clear, the latter essentially depends on the choice of metric. The *Wasserstein distance*  $W_2$  provides a suitable metric for measuring the regularity of a probability flow  $\mu_t$ , and it is known that the metric derivative of the flow  $\mu_t$  can be equivalently described by the  $L_2$ -norm  $\|v_t\|_{L_2(\mu_t)}$  of the corresponding velocity field  $v_t$ . It has been observed by the authors of [7] that a blow-up of this norm can raise severe problems for the neural network to approximate the flow, leading to issues like approximation errors or even mode collapse. Intriguingly, also diffusion models suffer from a velocity explosion at times close to the target, see [18].

This motivated us to establish a new physics-inspired model based on the *damped wave equation*, also known as the *telegrapher's equation*. This hyperbolic PDE models the evolution of a physical wave which gets dampened over time and travels with a finite fixed speed. It has been long known in the physics community that (mathematical) diffusion can be seen as the limit of the damped wave model with *infinite* damping and *infinite* propagation speed, and it has been found *unphysical* that particles in diffusion can travel with unbounded velocities, contradicting Einstein's principles of relativity. In contrast, our newly proposed *telegrapher's generative model* exhibits a favorable regularity with *bounded* velocities and a suitable long-term behavior. For sampling, we are able to utilize the flexible framework of flow matching, but applied to a stochastic process intrinsically connected to the telegrapher's equation, namely the *Kac process* [17], see Figure 1.

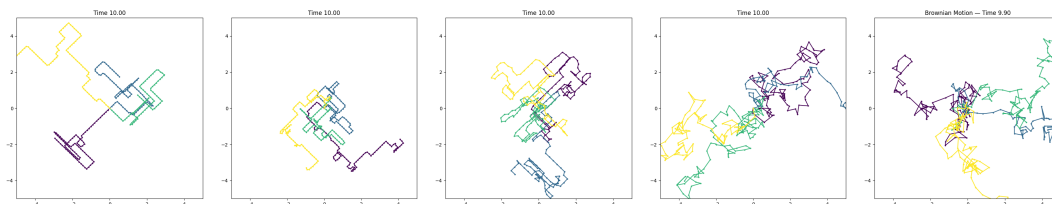


Figure 1: Paths of the componentwise Kac walk in 2D, simulated until time  $T = 10$  with damping/velocity parameters  $(a, c) = (1, 1), (2, 1), (4, 2), (25, 5)$ , and a standard Brownian motion (right).

## Contributions

1. We show that the Kac probability flow is a Lipschitz (hence absolutely) continuous curve in the Wasserstein space. In particular it fulfills the continuity equation with a bounded velocity field for which we determine a corresponding *conditional* velocity field for 1D flows starting in Dirac measures *analytically* (Theorem 4).
2. We revisit the connection to the telegrapher's equation and work out that the Kac flow converges to a diffusion flow for suitably related large damping and velocity coefficients, and also for large times (Theorem 8).

3. We extend the above regularity and convergence results to a multi-dimensional stochastic process which consists of independent 1D Kac processes in each spatial component (Proposition 10, Theorem 11). Moreover, we show that its conditional velocity field decomposes into univariate components (Theorem 13), and therefore obtain an *explicit* expression.
4. We use the *decomposed and explicitly given* conditional vector field to train a neural network to approximate the true velocity field using ideas from flow matching and an efficient sampling strategy for the Kac process. This decomposition method is generally applicable to other componentwise forward processes and velocity fields.
5. We implement our generative model and demonstrate its generation quality and scalability by numerical examples. In particular, we demonstrate its advantage over diffusion models in specific toy experiments.

**Outline of the paper.** Section 2 provides necessary preliminaries on curves in Wasserstein spaces. In Section 3 we explore the explosions of velocity fields of several popular neural flows which initially motivated us to study *different* (physics-inspired) flows. In Section 4 we examine the 1D Kac model, its relation to the telegrapher’s equation, and derive explicit formulas for the probability flow and conditional velocity field. A generalization to higher dimensions is provided in Section 5. Here we recall Kac’s insertion method connecting the 1D Kac process to the multi-dimensional telegrapher’s equation. Since the latter lacks a conservation of mass, we study a componentwise model in Subsection 5.2. An explicit representation of the velocity field of the multi-dimensional process is derived in Section 6. In Section 7, we use flow matching to approximate the corresponding velocity field and conduct numerical experiments.

## 2 Preliminaries: Curves in Wasserstein Spaces

Let  $\mathcal{P}_2(\mathbb{R}^d)$  denote the complete metric space of probability measures with finite second moments equipped with the Wasserstein distance

$$W_2^2(\mu, \nu) := \min_{\pi \in \Pi(\mu, \nu)} \int_{\mathbb{R}^d \times \mathbb{R}^d} \|x - y\|^2 d\pi(x, y),$$

where  $\Pi(\mu, \nu)$  denotes the set of all probability measures on  $\mathbb{R}^d \times \mathbb{R}^d$  having marginals  $\mu$  and  $\nu$ , called couplings or transport plans between  $\mu$  and  $\nu$ . The push-forward measure of  $\mu \in \mathcal{P}_2(\mathbb{R}^d)$  by a measurable map  $T : \mathbb{R}^d \rightarrow \mathbb{R}^d$  is defined by  $T_{\#}\mu := \mu \circ T^{-1}$ . Let  $I$  be a bounded interval in  $\mathbb{R}$ . The space  $AC^2(I; \mathcal{P}_2(\mathbb{R}^d))$  of *absolutely continuous* curves consists of all  $\mu_t : I \rightarrow \mathcal{P}_2(\mathbb{R}^d)$  for which there exists  $m \in L_2(I)$  such that

$$W_2(\mu_s, \mu_t) \leq \int_s^t m(r) dr \quad \text{for all } s \leq t, s, t \in I. \quad (1)$$

Here  $L_2(I)$  denotes the space of (equivalence classes of) square integrable real-valued function on an interval  $I$ . It is well known that a narrowly<sup>1</sup> continuous curve  $\mu_t : I \rightarrow \mathcal{P}_2(\mathbb{R}^d)$  belongs to

---

<sup>1</sup>In stochastic analysis, narrow convergence is also known as *weak convergence of measures*.

$AC^2(I; \mathcal{P}_2(\mathbb{R}^d))$ , iff there exists a Borel measurable vector field  $v : I \times \mathbb{R}^d \rightarrow \mathbb{R}^d$  such that  $(\mu_t, v_t)$  satisfies the *continuity equation*

$$\partial_t \mu_t + \nabla_x \cdot (\mu_t v_t) = 0 \quad (2)$$

in the sense of distributions and

$$\|v_t\|_{L_2(\mu_t)} \in L_2(I), \quad (3)$$

see [3, Definition 1.1.1; Theorem 8.3.1]. If in addition

$$\int_I \sup_{x \in B} \|v_t(x)\| + \text{Lip}(v_t, B) dt < \infty \quad \text{for all compact } B \subset \mathbb{R}^d, \quad (4)$$

then the *flow ODE*

$$\partial_t \varphi(t, x) = v_t(\varphi(t, x)), \quad \varphi(0, x) = x, \quad (5)$$

has a solution  $\varphi : I \times \mathbb{R}^d \rightarrow \mathbb{R}^d$  and  $\mu_t = \varphi(t, \cdot)_\# \mu_0$ , see [3, Proposition 8.1.8]. Note that often, absolutely continuous functions in  $AC^1(I; \mathcal{P}_2(\mathbb{R}^d))$  with  $m \in L_1(I)$  in (1) were considered in the literature. However, we need the stronger assumption of square integrability to define appropriate loss functions later.

Given an appropriate velocity field  $v_t$ , we can sample from a target distribution by starting in a sample  $x_0$  from the latent distribution and applying an ODE solver to (5). However, in this paper, we will reverse the flow direction by starting in the target distribution and ending (approximately) in the latent distribution at some final time  $t = T$ , similar to diffusion models. If we have access to the forward velocity  $v_t$ , then the reverse flow is simply given by the opposite velocity field  $-v_{T-t}$ .

### 3 Motivation

Our research was motivated by the explosion of velocity fields of certain flow models. If condition (4) or even worse the condition (3) is not fulfilled, we speak about an *exploding velocity field*. In the following, we give four examples of popular flows used in generative modeling. We denote the density (if it exists) of  $\mu_t$  by  $p_t$ , and we are occasionally imprecise when writing  $p_t = \mu_t$ .

**1. Flows from couplings.** Learning absolutely continuous curves induced by couplings of the latent and target measure is a task addressed in *flow matching*, see [21], and for an overview, [43]. Let us consider the latent  $\mu_0 = \mathcal{N}(0, I_d) dx$  and the target distribution  $\mu_1 = \delta_0$ , and their independent coupling  $\alpha := \mu_0 \times \mu_1$ . Then the curve  $\mu_t := e_{t,\#} \alpha$  with  $e_t = (1-t)x + ty$  admits the density

$$p_t(x) = (2\pi(1-t)^2)^{-\frac{d}{2}} e^{-\frac{\|x\|^2}{2(1-t)^2}}, \quad t \in I = [0, 1)$$

and with the so-called velocity field induced by  $\alpha$ ,

$$v_t(x) = \nabla \left( \frac{1-t}{t} \log p_t(x) + \frac{1}{2t} \|x\|^2 \right) = -\frac{x}{1-t}, \quad (6)$$

see [43, Example 4.12], it fulfills the continuity equation (2). Unfortunately, (4) is *not* fulfilled due to the singularity at  $t = 1$ . Nevertheless, the trajectory  $\varphi_t$  of the ODE (5) is given by

$$\varphi_t(x) = (1-t)x,$$

and therefore it holds  $v_t(\varphi_t(x)) = -x$ . Hence, we have a constant velocity field along the curve, and by switching to spherical coordinates we see that

$$\|v_t\|_{L_2(p_t)}^2 = \int_{\mathbb{R}^d} \|v_t(\varphi_t(x))\|^2 dp_0(x) = \int_{\mathbb{R}^d} \|x\|^2 dp_0(x) = d,$$

such that (3) is still valid.

**2. Diffusion flows.** *Diffusion models* or *score-based models* are based on the Fokker-Planck equation of the Wiener process or Ornstein-Uhlenbeck process, which is the diffusion equation (with drift), see e.g. [37]. Let us consider the probability flow  $p_t$  solving the standard diffusion equation

$$\partial_t p_t = \frac{\sigma^2}{2} \nabla \cdot (p_t \nabla \log p_t) = \frac{\sigma^2}{2} \Delta p_t, \quad t \in (0, 1], \quad \lim_{t \downarrow 0} p_t = \delta_0,$$

starting in the target  $\delta_0$  given by a Dirac distribution at 0. Here, the limit for  $t \downarrow 0$  is taken in the sense of distributions and  $\frac{\sigma^2}{2}$  is the diffusion constant. The solution is analytically given by

$$p_t(x) = (2\pi\sigma^2 t)^{-\frac{d}{2}} e^{-\frac{\|x\|^2}{2\sigma^2 t}}, \quad t \in (0, 1].$$

We choose  $\sigma^2 = 1$  such that the latent is  $p_1 = \mathcal{N}(0, I_d)$ . The velocity field is  $v_t(x) = \frac{x}{2t}$ . After the reparameterization  $\tilde{p}_t = p_{1-t}$ , the reverse flow reads as

$$\tilde{p}_t(x) = (2\pi(1-t))^{-\frac{d}{2}} e^{-\frac{\|x\|^2}{2(1-t)}}, \quad t \in I = [0, 1], \quad \tilde{p}_0 = \mathcal{N}(0, I_d),$$

and satisfies  $\tilde{p}_1 = \delta_0$  in a distributional sense. The reverse velocity field is given by

$$\tilde{v}_t(x) = -\frac{x}{2(1-t)}, \quad (7)$$

and the reverse trajectory  $\tilde{\varphi}_t$  solving the ODE (5) by

$$\tilde{\varphi}_t(x) = x\sqrt{1-t}.$$

Here it holds  $\tilde{v}_t(\tilde{\varphi}_t(x)) = -\frac{x}{2\sqrt{1-t}}$ . Thus, again by switching to spherical coordinates, we see that

$$\|\tilde{v}_t\|_{L_2(\tilde{p}_t)}^2 = \int_{\mathbb{R}^d} \|\tilde{v}_t(\tilde{\varphi}_t(x))\|^2 d\tilde{p}_0(x) = \frac{d}{4(1-t)}, \quad (8)$$

so that both conditions (3) and (4) are violated, and  $\tilde{p}_t \notin AC^2([0, 1]; \mathcal{P}_2(\mathbb{R}))$ .

In practice, instability issues concerning the learning of  $\tilde{v}_t$  are caused by this explosion at times close to the target, and need to be avoided by e.g. *time truncations*, see e.g. [18].

For a heuristic analysis also including drift-diffusion flows, we refer to [33].

**3. Flows from linear interpolation of Boltzmann energies.** For Boltzmann densities  $p_t = e^{-f_t}/Z_t$ , where  $Z_t := \int e^{-f_t} dx$ , straightforward computation gives the Rao-Fisher differential equation

$$\partial_t p_t = -(\partial_t f_t - \mathbb{E}_{p_t}[\partial_t f_t]) p_t.$$

Since on the other hand, the continuity equation becomes

$$\partial_t p_t = \nabla \cdot (p_t v_t) = (-\langle \nabla f_t, v_t \rangle + \nabla \cdot v_t) p_t,$$

the vector field has to fulfill

$$\partial_t f_t - \mathbb{E}_{p_t}[\partial_t f_t] = -\langle \nabla f_t, v_t \rangle + \nabla \cdot v_t. \quad (9)$$

Sampling of unnormalized target Boltzmann densities  $p_1$  often uses the geometric density interpolation  $p_t = p_0^{1-t} p_1^t$  which corresponds to the *linear interpolation*  $f_t = (1-t)f_0 + t f_1$ . Then (9) reads as

$$f_1 - f_0 - Z_t + \langle \nabla f_t, v_t \rangle - \nabla \cdot v_t = 0,$$

where  $Z_t$  is the normalization constant. There are a variety of approaches for approximating the vector field corresponding to the linear interpolation, see, e.g., [26, 30] for kernel-based methods. However, for certain asymmetric constellations of prior and target measure, a mode collapse of the neural model was numerically observed in [27]. Indeed, it was analytically shown in [7] that for the Laplacian  $p_0 \propto e^{-|x|}$  centered at 0 and a Laplacian-like target distribution  $p_1 \propto e^{-2 \min\{|x|, |x-m|\}}$  with a mode at 0 and a second one at  $m > 0$ , the velocity norm grows exponentially with  $m$ , i.e.  $\|v_1\|_{L_2(p_1)}^2 \gtrsim e^{\alpha m}$ . Using Gaussian mixtures instead of Laplacians, an explosion of the type  $\int_0^1 \|v_t\|_{L_2(p_t)}^2 dt \gtrsim m^4 e^{\alpha m^2}$  was proven in [12, Proposition 9].

Note that replacing the linear interpolation by a more flexible variant with an additional learnable quantity, the mode collapse was numerically avoided in [27]. For an approach to (9) from the control theory point of view that leverages the explosion effect, we refer to [10, 4, 39].

**4. Poisson flows.** In [44], another physics-inspired generative model was proposed using the Poisson equation on  $\mathbb{R}^d$  augmented by an additional dimension  $z$ :

$$-\Delta \varphi(x, z) = p_{\text{data}}(x) \delta_0(z), \quad x \in \mathbb{R}^d, z \in \mathbb{R}.$$

Here, the target distribution  $p_{\text{data}}$  is interpreted as electrical charges on the  $z = 0$  hyperplane describing an electric field  $\varphi$ . The time-independent, but  $z$ -dependent velocity field  $v(x, z) = -\nabla \varphi(x, z)$  then determines the particle trajectories through the  $(d+1)$ -dimensional space. This augmentation has been found crucial for the model to work properly, but has the following explosion of the velocity field as a consequence: the Poisson velocity field  $v(x, z)$  has the analytical expression

$$v(x, z) = \frac{1}{S_d} \int_{\mathbb{R}^{d+1}} \frac{(x, z) - (y, z')}{\|(x, z) - (y, z')\|^{d+1}} p_{\text{data}}(y) \delta_0(z') dy dz', \quad (10)$$

where  $S_d$  is the surface area of the  $d$ -sphere. For the uniform distribution  $p_{\text{data}}$  on  $[0, 1]^d$ , this results for any  $x \in [0, 1]^d$  and  $z = 0$  in

$$\int_{\mathbb{R}^{d+1}} \left\| \frac{(x, 0) - (y, z')}{\|(x, 0) - (y, z')\|^{d+1}} p_{\text{data}}(y) \delta_0(z') \right\| dy dz' = \int_{[0, 1]^d} \frac{1}{\|x - y\|^d} dy = \infty. \quad (11)$$

Hence, the Poisson field (10) might not be well-defined on the support of the target distribution, and can get arbitrarily large around it. Notice how the augmentation by  $z$  causes this explosion (11), while in the non-augmented case the corresponding integral stays finite.

Similarly to the diffusion case, the explosion (11) at heights  $z$  close to the data ( $z = 0$ ) makes suitable *truncations* necessary when approximating the velocity field by a neural network, see [44, Ch. 3.2].

In the next sections, we introduce a physics-inspired generative model based on the damped wave equation which does not suffer from exploding velocity fields.

## 4 Telegrapher's Equation and Kac Model in 1D

In [22], it was contemplated to consider other physics-inspired models next to above diffusion (parabolic) and Poisson (elliptic) equations for generative modeling. Here, we want to further pursue this idea and focus on a process related to the *telegrapher's equation*, also known as *damped wave equation*. This is a linear hyperbolic PDE of the form

$$\begin{aligned} \partial_{tt}u(t, x) + 2a \partial_t u(t, x) &= c^2 \partial_{xx}u(t, x), & x \in \mathbb{R}, t > 0, \\ u(0, x) &= f_0(x), \\ \partial_t u(0, x) &= 0. \end{aligned} \tag{12}$$

Here,  $a > 0$  is the damping coefficient, and  $c > 0$  describes the velocity of the wave front. Historically, the equation (12) originates from the modeling of voltage and current in electrical transmission lines (telegraphs). It is known that if the damping  $a$  and velocity  $c$  go suitably to infinity, see Remark 9, then the diffusion model is retrieved. Hence, diffusion can be seen as "*an infinitely  $a$ -damped wave with infinite propagation speed  $c$* ". The idea of particles traveling with infinite speed has already encountered resistance in the physics community [6, 42, 9, 40], since it violates Einstein's laws of relativity. But also in the field of generative modeling, this can be seen as a reason for the explosion of velocity fields of diffusion models. Hence, if we restrict ourselves to above model (12), where waves travel only with *finite* speed  $c$ , we expect the velocity field  $v_t$  to behave well. Indeed, we will show that the telegrapher's model does not admit a velocity explosion, but shares the same long-time asymptotics as diffusion.

Of central importance for the theoretical analysis and for generative modeling is the stochastic representation of (12) given by Kac [17] which we recall next.

### 4.1 Kac Flow in 1D

Suppose that a particle starts at  $x_0 = 0$  and always moves with velocity  $c > 0$  in either positive or negative direction. The initial direction is determined by a random symmetric coin-flip. Each step is of duration  $\Delta t$  and therefore we have  $\Delta x = c\Delta t$ . A particle continues to move in the same direction with probability  $1 - a\Delta t$ , and reverses with the probability  $a\Delta t$ , where  $a > 0$  is a fixed parameter. Intuitively, for small  $\Delta t$  the particle tends to move in the same direction (resembling some form of inertia in the movement), until it collides with some obstacle and reverses its direction.

For  $n \in \mathbb{N}$ , we consider a random variable  $S_n$  taking the possible displacement of a particle after  $n$  steps as values. Let us first consider the case that the initial direction is positive, so that  $S_0 = c\Delta t$ , where we consider this as step 0. Then we have

$$S_n = c\Delta t(1 + \varepsilon_1 + \varepsilon_1\varepsilon_2 + \dots + \varepsilon_1 \dots \varepsilon_n),$$

where  $\varepsilon_k$  are random variables taking the value  $-1$  with probability  $a\Delta t$  and  $1$  with probability  $1 - a\Delta t$ , or alternatively

$$S_n = c\Delta t \sum_{k=0}^n (-1)^{N_k}, \quad (13)$$

where  $N_0 = 0$  and  $N_k \sim B(k, a\Delta t)$ ,  $k \in \mathbb{N} \setminus \{0\}$ , are the binomially distributed random variables denoting the number of direction changes within step 1 to  $k$ . We consider the continuous limit of this discrete process as  $n \rightarrow \infty$ ,  $\Delta t \rightarrow 0$  such that  $na\Delta t \rightarrow at$ . Then it is well known that  $N_n$  converges (in distribution) to the Poisson distribution  $\text{Poi}(at)$  with expectation value  $at$ . The number of reversals up to time  $t$  is given by a homogeneous *Poisson point process*  $(N(t))_{t \geq 0}$  with rate  $a$ , i.e.,

- i)  $N(0) = 0$ ;
- ii) The increments of  $N(t)$  are independent, i.e. for every  $m \in \mathbb{N}$  and all  $0 \leq t_0 < t_1 < \dots < t_m$  the random variables  $N(t_1) - N(t_0)$ ,  $N(t_2) - N(t_1)$ ,  $\dots$ ,  $N(t_m) - N(t_{m-1})$  are independent;
- iii)  $N(t) - N(s) \sim \text{Poi}(a(t-s))$  for all  $0 \leq s < t$ .

Then the corresponding particle displacement and continuous analogue of (13) is given by

$$S(t) = c\tau_t \quad \text{with} \quad \tau_t := \int_0^t (-1)^{N(s)} ds. \quad (14)$$

We refer to  $\tau_t$  as *random time*. Finally, for a (symmetrically) random initial direction, the displacement at time  $t$  is determined by the *Kac process starting in 0*,

$$K(t) := B_{\frac{1}{2}} S(t) = B_{\frac{1}{2}} c \tau_t, \quad (15)$$

where  $B_{\frac{1}{2}} \sim B(1, \frac{1}{2})$  is a Bernoulli random variable taking the values  $\pm 1$ . Naturally, for a random variable  $X_0$  we call

$$X_t := X_0 + K(t) = X_0 + B_{\frac{1}{2}} S(t) \quad (16)$$

the *Kac process starting in  $X_0$* .

## 4.2 Relation of Kac' Flow to 1D Telegrapher's Equation

Similar to the case of Brownian motions and diffusion equations, there is a Feynman-Kac type relation between the Kac process and the telegrapher's equation in 1D. Let  $H^2(\mathbb{R})$  denote the space of two times weakly differentiable functions with derivatives in  $L_2(\mathbb{R})$ .

**Theorem 1.** *For any initial function  $f_0 \in H^2(\mathbb{R})$ , the function*

$$u(t, x) = \frac{1}{2} \mathbb{E} \left[ f_0(x + S(t)) \right] + \frac{1}{2} \mathbb{E} \left[ f_0(x - S(t)) \right] \quad (17)$$

*solves the 1D telegrapher's equation (12).*

*Further, if  $f_0$  is a probability density of a random variable  $X_0$  independent of  $S(t)$ , then (17) is the probability density of the Kac process  $(X_t)_{t \geq 0}$  starting in  $X_0 \sim f_0$  defined by (16).*

*Proof.* The first part of claim was originally conjectured by Kac [17] and proven in [16] using martingales. For the second part, note that the Kac process starting in  $X_0 \sim f_0$  with initial positive direction is given by  $X_0 + S(t)$  and with initial negative direction by  $X_0 - S(t)$ . Then we obtain with the usual push-forward  $P_{S(t)} := S(t)_\# \mathbb{P}$  that

$$\begin{aligned} \mathbb{E}[f_0(x - S(t))] &= \int_{\Omega} f_0(x - S(t)(\omega)) \, d\mathbb{P}(\omega) = \int_{S(t)(\Omega)} f_0(x - y) \, dP_{S(t)}(y) \\ &= (f_0 * P_{S(t)})(x) = p_{X_0 + S(t)}(x), \end{aligned}$$

where we have used the independence of  $X_0$  and  $S(t)$  in the last equality. Similarly, we get

$$\mathbb{E}[f_0(x + S(t))] = (f_0 * P_{-S(t)})(x) = p_{X_0 - S(t)}(x).$$

Hence, it follows  $u(t, x) = \frac{1}{2}(p_{X_0 + S(t)}(x) + p_{X_0 - S(t)}(x)) = p_{X_0 + B_{\frac{1}{2}}S(t)}(x)$  by the law of total probability.  $\square$

By the next lemma, there is an analytic representation of the distributional solution of the telegrapher's equation (12). We refer to [29] and [25] for the proof via distributions. For a characterization of measures as (tempered) distributions, see also [34, Chapter 4.4].

**Lemma 2.** *The telegrapher's equation (12) starting in a generalized function (distribution)  $f_0$  has the distributional solution*

$$\begin{aligned} u(t, x) &= \frac{1}{2}e^{-at} \left( f_0(x + ct) + f_0(x - ct) + \beta ct \int_{x-ct}^{x+ct} \frac{I'_0(\beta r_t(x-y))}{r_t(x-y)} f_0(y) \, dy \right. \\ &\quad \left. + \beta \int_{x-ct}^{x+ct} I_0(\beta r_t(x-y)) f_0(y) \, dy \right), \end{aligned} \tag{18}$$

where

$$r_t(x) := \sqrt{c^2 t^2 - x^2}, \quad \beta := \frac{a}{c},$$

and  $I_k$  denotes the  $k$ -th modified Bessel function of first kind. (Note that  $I'_0 = I_1$ .)

In particular, for the Dirac distribution  $f_0 = \delta_0$  in zero, it holds

$$u(t, x) = \frac{1}{2}e^{-at} (\delta_0(x + ct) + \delta_0(x - ct)) + \tilde{u}(t, x), \tag{19}$$

where

$$\tilde{u}(t, x) := \frac{1}{2}e^{-at} \left( \beta ct \frac{I'_0(\beta r_t(x))}{r_t(x)} + \beta I_0(\beta r_t(x)) \right) 1_{[-ct, ct]}(x). \tag{20}$$

This distribution is associated to a probability measure  $\mu_t$  with an atomic part given by the Dirac measures  $\delta_{-ct}, \delta_{ct}$  and an absolutely continuous part  $\tilde{u}(t, \cdot)$ , i.e.

$$\mu_t(A) = \frac{e^{-at}}{2} (\delta_{-ct}(A) + \delta_{ct}(A)) + \int_A \tilde{u}(t, x) \, dx \quad \text{for all Borel sets } A \subset \mathbb{R}.$$

The measure  $\mu_t$  is exactly the probability distribution of the Kac process  $K(t)$  starting in 0 from (15), see [15, Section 2].

Note that the Kac process  $K(t)$  starting in 0 does not admit a density itself. The following remark states an important relation with the left- and right moving Kac processes.

**Remark 3.** *By [15, Section 2], the absolute continuous part of the distribution of the initially right-moving and initially left-moving Kac process  $\pm S(t)$  starting in 0 is given by*

$$\tilde{u}_{\pm}(t, x) = \frac{1}{2} e^{-at} \left( \frac{\beta(ct \pm x)}{r_t(x)} I'_0(\beta r_t(x)) + \beta I_0(\beta r_t(x)) \right) 1_{[-ct, ct]}(x),$$

respectively, and it holds  $\tilde{u} = \frac{1}{2}(\tilde{u}_+ + \tilde{u}_-)$  with  $\tilde{u}$  in (20). By [17, Eq. (12) & (11)], the marginal densities  $\tilde{u}_{\pm}$  satisfy the PDEs

$$\partial_t \tilde{u}_+ + c \partial_x \tilde{u}_+ = -a \tilde{u}_+ + a \tilde{u}_-, \quad \partial_t \tilde{u}_- - c \partial_x \tilde{u}_- = a \tilde{u}_+ - a \tilde{u}_-. \quad (21)$$

Intuitively, the equations (21) can be understood as the continuity equation for the right-moving and left-moving particles including source and sink terms, see [32]. Adding the equations yields

$$\partial_t(\tilde{u}_+ + \tilde{u}_-) + c \partial_x(\tilde{u}_+ - \tilde{u}_-) = 0.$$

Thus, with the continuous flux

$$\tilde{J}(t, x) := \frac{c}{2} (\tilde{u}_+(t, x) - \tilde{u}_-(t, x)) = \frac{1}{2} e^{-at} \frac{\beta c x}{r_t(x)} I'_0(\beta r_t(x)), \quad x \in (-ct, ct). \quad (22)$$

we arrive at the continuity equation

$$\partial_t \tilde{u} + \partial_x \tilde{J} = 0. \quad (23)$$

◇

After these preparations, we can explicitly describe the velocity field of the Kac process starting in a Dirac point which will be important for learning velocity fields later. The Kac velocity in (25) may be compared with those of coupling and diffusion flows given in (6) and (7), respectively.

**Theorem 4.** *Let  $f_0 = \delta_0$  be the Dirac measure on  $\mathbb{R}$ . Then  $\mu_t$  associated to  $u(t, \cdot)$  in (19) solves the continuity equation*

$$\partial_t \mu_t = -\partial_x(\mu_t v_t) \quad (24)$$

in a weak sense, where the velocity field  $v_t(x) = v(t, x)$  is given by

$$v(t, x) := \begin{cases} \frac{x}{t + \frac{r_t(x)}{c}} \frac{I'_0(\beta r_t(x))}{I'_0(\beta r_t(x))} & \text{if } x \in (-ct, ct), \\ c & \text{if } x = ct, \\ -c & \text{if } x = -ct, \\ \text{arbitrary} & \text{otherwise.} \end{cases} \quad (25)$$

*Proof.* At this time, we will assume the existence of a velocity field  $v_t$  satisfying the continuity equation (24) in a weak sense, and show that in this case  $v_t$  must admit the form (25). Later, in Proposition 10, we generally and independently prove that  $\mu_t$  is indeed absolutely continuous and admits a velocity field  $v_t$ .

Fix  $t > 0$ . Formal differentiation of (19) leads to

$$\begin{aligned} \partial_t u(t, x) &= -au(t, x) + \frac{1}{2}e^{-at}(c\delta'_0(x+ct) - c\delta'_0(x-ct)) \\ &\quad + (a + a^2t)z_1(t, x) + atz_2(t, x)1_{[-ct, ct]}(x), \end{aligned} \quad (26)$$

where

$$z_1(t, x) := \frac{I'_0(\beta r_t(x))}{r_t(x)} \quad \text{and} \quad z_2(t, x) := \frac{act I''_0(\beta r_t(x)) - c^2t z_1(t, x)}{r_t(x)^2}.$$

First, we consider the case  $x \in (-ct, ct)$ . Then, all the Dirac terms disappear and we only need to work with  $\tilde{u}$  given in (20), and  $\partial_t \tilde{u}$  is given in (26) without the Dirac terms. Using l' Hospital's rule and  $I'_0(0) = I_0^{(3)}(0) = 0$ ,  $I_0''(0) = \frac{1}{2}$ ,  $I_0^{(4)}(0) = \frac{3}{8}$ , it is easy to check that both functions  $z_1, z_2$  are bounded in  $x \in (-ct, ct)$ , so that  $\partial_t \tilde{u}(t, \cdot)$  is integrable. Since  $\tilde{u}(t, x)$  is symmetric with respect to  $x$ , the velocity  $v(t, x)$  must be antisymmetric in  $x$ . By (24), we conclude

$$2\tilde{u}(t, x)v(t, x) = -\int_{-x}^x \partial_t \tilde{u}(t, y) dy \quad \text{for all } x \in (-ct, ct). \quad (27)$$

At the same time, we obtain from (23) and by the anti-symmetry of  $\tilde{J}(t, \cdot)$  that

$$-\int_{-x}^x \partial_t \tilde{u}(t, y) dy = \int_{-x}^x \partial_x \tilde{J}(t, y) dy = 2\tilde{J}(t, x) \quad \text{for all } x \in (-ct, ct).$$

Together with (27), (22) and (20), this implies

$$v(t, x) = \frac{\tilde{J}(t, x)}{\tilde{u}(t, x)} = \frac{e^{-at} \frac{\beta cx}{r_t(x)} I'_0(\beta r_t(x))}{e^{-at} \left[ \frac{\beta ct}{r_t(x)} I'_0(\beta r_t(x)) + \beta I_0(\beta r_t(x)) \right]} = \frac{x}{t + \frac{r_t(x)}{c} \frac{I_0(\beta r_t(x))}{I'_0(\beta r_t(x))}},$$

which shows (25) for all  $x \in (-ct, ct)$ .

Next, we consider the case  $x = \pm ct$ . For any test function  $\phi \in C_c^\infty(\mathbb{R})$ , we get

$$\begin{aligned} \int_{-\infty}^{\infty} \partial_t u(t, x) \phi(x) dx &= -\frac{ae^{-at}}{2}(\phi(-ct) + \phi(ct)) + \frac{e^{-at}}{2}(-c\phi'(-ct) + c\phi'(ct)) \\ &\quad + \int_{-ct}^{ct} \partial_t \tilde{u}(t, x) \phi(x) dx. \end{aligned}$$

On the other hand, the continuity equation (24) gives

$$\begin{aligned} \int_{-\infty}^{\infty} \partial_t u(t, x) \phi(x) dx &= \int_{-\infty}^{\infty} -\partial_x(u(t, x)v(t, x)) \phi(x) dx = \int_{-\infty}^{\infty} u(t, x)v(t, x) \phi'(x) dx \\ &= \frac{e^{-at}}{2}(v(t, -ct)\phi'(-ct) + v(t, ct)\phi'(ct)) + \int_{-ct}^{ct} \tilde{u}(t, x)v(t, x) \phi'(x) dx. \end{aligned}$$

Now we can choose a sequence of test functions  $\phi_n \in C_c^\infty(\mathbb{R})$  such that  $\phi_n \equiv 0$  on  $[-ct + \frac{1}{n}, ct - \frac{1}{n}]$ ,  $\|\phi_n\|_\infty < \frac{1}{n}$ ,  $\phi'_n(ct) = 1$  and  $\phi'_n(-ct) = -1$ . Then the anti-symmetry  $v(t, -ct) = -v(t, ct)$  and above identities in the limit  $n \rightarrow \infty$  yield

$$\frac{e^{-at}}{2}(-c \cdot (-1) + c \cdot 1) = \frac{e^{-at}}{2}(-v(t, ct) \cdot (-1) + v(t, ct) \cdot 1),$$

and hence,  $v(t, ct) = c$ . By anti-symmetry, it holds  $v(t, -ct) = -c$ , and the proof of (25) is finished.  $\square$

## 5 Multi-dimensional Generalizations of the Telegrapher's Model

The connection between the telegrapher's equation and the Kac process can be generalized to higher dimensions via Kac's insertion method which we briefly describe in Subsection 5.1. In contrast to one dimension, initial probability densities do not remain probability densities in the PDE formulation. Yet, we state a convergence result towards diffusion, which we will use subsequently. To circumvent the lack of conservation of mass, we propose a componentwise extension to higher dimensions in Subsection 5.2, and we prove regularity and convergence results of our componentwise process.

### 5.1 Kac's Insertion Method

A generalization of Theorem 1 to multiple dimensions is given by the following theorem.

**Theorem 5.** *For any initial function  $f_0 \in H^2(\mathbb{R}^d)$ ,  $d \geq 1$ , let  $w_c(t, x)$  be the solution of the undamped wave equation with velocity  $c > 0$  given by*

$$\begin{aligned} \partial_{tt}w(t, x) &= c^2 \Delta w(t, x), & x \in \mathbb{R}^d, t > 0, \\ w(0, x) &= f_0(x), \\ \partial_t w(0, x) &= 0. \end{aligned} \tag{28}$$

Then, the function  $u : [0, \infty) \times \mathbb{R}^d \rightarrow \mathbb{R}$  defined by

$$u(t, x) := \mathbb{E}[w_c(\tau_t, x)] \tag{29}$$

solves the multi-dimensional damped wave equation

$$\begin{aligned} \partial_{tt}u(t, x) + 2a \partial_t u(t, x) &= c^2 \Delta u(t, x), & x \in \mathbb{R}^d, t > 0, \\ u(0, x) &= f_0(x), \\ \partial_t u(0, x) &= 0. \end{aligned} \tag{30}$$

This claim was again conjectured in [17] and a proof was given in [11, Theorem 4] using semigroup theory.

**Remark 6.** *In 1D, the solution of (28) is given by  $w_c(t, x) = \frac{1}{2}(f_0(x + ct) + f_0(x - ct))$ , so that (29) reproduces (17). Unfortunately, in higher dimensions, the telegrapher's solution (29) might not stay a probability density anymore. For example, the mass  $\int_{\mathbb{R}^3} u(t, x) dx$  in 3D behaves like  $1 - e^{-t}$ , see [40, Ch. 2.2].*  $\diamond$

Nevertheless, we will see that using an analogous insertion method for the diffusion, it is possible to show that the diffusion and telegrapher's solutions converge to each other.

Recall that a Wiener process (Brownian motion)  $\mathbf{W} = (\mathbf{W}(t))_{t \geq 0}$ ,  $\mathbf{W}(t) \in \mathbb{R}^d$ ,  $d \geq 1$ , is characterized by i)  $\mathbf{W}(0) = \mathbf{0}$ , ii) independent increments, iii)  $\mathbf{W}(t) - \mathbf{W}(s) \sim \mathcal{N}(0, (t-s)I_d)$  for all  $0 \leq s < t$ , and iv)  $\mathbf{W}$  is almost surely continuous in  $t$ . From now on, we emphasize vector-valued quantities using bold letters.

**Lemma 7.** For  $f_0 \in H^2(\mathbb{R}^d)$ , let  $w$  be the solution of the undamped wave equation (28) with  $c = 1$ . Let  $W$  be a one-dimensional Wiener process. Then

$$h(t, x) := \mathbb{E}[w(\sigma W(t), x)], \quad \sigma > 0, \quad (31)$$

solves the heat equation

$$\begin{aligned} \partial_t h(t, x) &= \frac{\sigma^2}{2} \Delta h(t, x), \quad x \in \mathbb{R}^d, \quad t > 0, \\ h(0, x) &= f_0(x). \end{aligned} \quad (32)$$

The statement can be found in [15], and a proof was given in [11, Theorem 5].

Note that if  $f_0$  is a probability density and  $\mathbf{X}_0 \sim f_0$ , then  $h$  given by (31) is the probability density of a  $d$ -dimensional Wiener process  $\sigma \mathbf{W}(t)$  starting in  $\mathbf{X}_0$ . Interestingly the functions  $h$  and  $u$  converge to each other for  $t \rightarrow \infty$ .

**Theorem 8.** Fix  $c_0 > 0$ . For  $f_0 \in H^2(\mathbb{R}^d)$ , let  $u$  be given by (29) with  $a > 0$ ,  $c \geq c_0$ , and  $h$  by (31) with  $\sigma^2 := \frac{c^2}{a}$ . Then there exists a constant  $C = C(c_0, d)$  such that

$$\|h(t, \cdot) - u(t, \cdot)\|_{L_2(\mathbb{R}^d)} \leq C \left( \frac{1}{at} + \frac{1}{c(ta)^{\frac{1}{2}}} \right) \quad \text{for all } t > 0. \quad (33)$$

*Proof.* It is well-known that the Laplacian  $\Delta : H^2(\mathbb{R}^d) \subset L_2(\mathbb{R}^d) \rightarrow L_2(\mathbb{R}^d)$  is a self-adjoint linear operator with non-positive spectrum  $\sigma(\Delta) = (-\infty, 0]$ . By [23, Corollary 2] the solution of (28) with  $c = 1$  is given by  $w(t, \cdot) = C(t)f_0$ , where  $(C(t))_{t \geq 0}$  is a uniformly bounded so-called cosine operator function with  $\|C(t)\|_{L_2 \rightarrow L_2} \leq 1$  for all  $t \geq 0$ . In particular, it follows that  $\|w(t, \cdot)\|_{L_2(\mathbb{R}^d)} \leq \|f_0\|_{L_2(\mathbb{R}^d)}$  is uniformly bounded in  $t$ . Now, [15, Theorem 2] yields the claim.  $\square$

**Remark 9.** By (33), we see that for any  $t \geq 0$ , the solution  $u^{a,c}(t, \cdot)$  of the telegrapher's equation (30) converges to the solution  $h(t, \cdot)$  of the diffusion equation (32) for  $a, c \rightarrow \infty$  with fixed  $\sigma^2 = \frac{c^2}{a}$ .  $\diamond$

## 5.2 Multi-Dimensional Kac Process

For generative modeling, we propose to circumvent the missing conservation of mass of the multi-dimensional telegrapher's equation (30), see Remark 6, by using a multivariate random process which consists of independent 1D Kac processes in each spatial component.

For a random variable  $\mathbf{X}_0 \in \mathbb{R}^d$ ,  $d \geq 1$ , we consider i.i.d.<sup>2</sup> copies  $K^i(t)$ ,  $i = 1, \dots, d$ , of a Kac process (15) starting in  $\mathbf{0}$ . Then, we call

$$\mathbf{K}(t) := (K^1(t), \dots, K^d(t)) \quad (34)$$

a  $d$ -dimensional Kac process starting in  $\mathbf{0} \in \mathbb{R}^d$ , and

$$\mathbf{X}_t := \mathbf{X}_0 + \mathbf{K}(t)$$

the respective Kac process starting in  $\mathbf{X}_0$ .

The stepwise linear movement of the Kac process  $(\mathbf{X}_t)_{t \geq 0}$  translates into a favorable regularity of its probability flow  $(P_{\mathbf{X}_t})_t$ . In particular, it is absolutely continuous in the Wasserstein space  $\mathcal{P}_2(\mathbb{R}^d)$  and there is no local explosion of the velocity field as in (8).

<sup>2</sup>We use i.i.d. Kac processes just for simplicity. But our framework also allows for independent processes  $K_i$  each with their own parameters  $(a_i, c_i)$ .

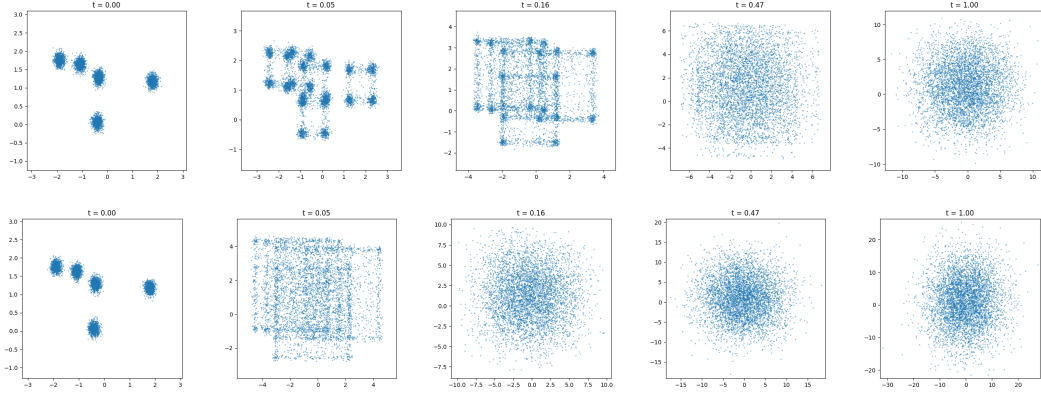


Figure 2: The distribution of the Kac process  $\mathbf{X}_t$  starting in a 2D Gaussian mixture, simulated until time  $T = 10$  with  $(a, c) = (1, 1)$  (upper row) and  $(a, c) = (5, 5)$  (lower row).

**Proposition 10.** *Let  $P_{\mathbf{X}_0} \in \mathcal{P}_2(\mathbb{R}^d)$ . Then, for the probability distribution flow  $(\mu_t)_{t \geq 0} := (P_{\mathbf{X}_t})_{t \geq 0}$  of the  $d$ -dimensional Kac process  $\mathbf{X}_t$  starting in  $\mathbf{X}_0$ , the following holds true:*

- i)  $(\mu_t)_{t \geq 0}$  is Lipschitz continuous in the Wasserstein space  $(\mathcal{P}_2(\mathbb{R}^d), W_2)$  with constant  $d^{\frac{1}{2}}c$ , and  $\mathbf{X}_t$  is almost surely Lipschitz continuous in  $\mathbb{R}^d$  with the same constant.*
- ii)  $(\mu_t)_{t \geq 0}$  is an absolutely continuous curve in  $AC^2([0, T]; \mathcal{P}_2(\mathbb{R}^d))$  for any  $T > 0$ , and admits a velocity field fulfilling*

$$\|v_t\|_{L^2(\mu_t)}^2 \leq dc^2 \quad \text{for a.e. } t \in [0, \infty), \quad (35)$$

- iii) The support of  $(\mu_t)_{t \geq 0}$  grows at most linearly in time.*

*Proof.* i) Fix  $0 \leq s < t$ . By construction of  $\mathbf{X}_t$  via (14), we obtain for  $\mathbb{P}$ -a.e.  $\omega$  that

$$\begin{aligned} \|\mathbf{X}_t(\omega) - \mathbf{X}_s(\omega)\|^2 &= \|\mathbf{K}(t)(\omega) - \mathbf{K}(s)(\omega)\|^2 = \sum_{i=1}^d |K_i(t)(\omega) - K_i(s)(\omega)|^2 \\ &= \sum_{i=1}^d \left| c B_{\frac{1}{2}}(\omega) \int_s^t (-1)^{N(z)(\omega)} dz \right|^2 \\ &\leq dc^2 |t - s|^2. \end{aligned} \quad (36)$$

This shows that  $\mathbf{X}_t$  is almost surely Lipschitz continuous in  $\mathbb{R}^d$  with constant  $d^{\frac{1}{2}}c$ .

Now, we consider the canonical transport plan  $\pi : \mathbb{R}^d \times \mathbb{R}^d \rightarrow \mathbb{R}$  defined by  $\pi(B) := \mathbb{P}((\mathbf{X}_s, \mathbf{X}_t) \in B)$  for all Borel measurable  $B \in \mathcal{B}(\mathbb{R}^d \times \mathbb{R}^d)$ . Indeed, it holds  $\pi(A \times \mathbb{R}^d) = P_{\mathbf{X}_s}(A)$  and  $\pi(\mathbb{R}^d \times A) = P_{\mathbf{X}_t}(A)$  for all  $A \in \mathcal{B}(\mathbb{R}^d)$ . Furthermore, we have  $\pi \in \mathcal{P}_2(\mathbb{R}^d \times \mathbb{R}^d)$ : it holds that

$$\begin{aligned} \int_{\mathbb{R}^d \times \mathbb{R}^d} \|(x, y)\|^2 d\pi(x, y) &= \int_{\Omega \times \Omega} \|(\mathbf{X}_0 + \mathbf{K}(s), \mathbf{X}_0 + \mathbf{K}(t))\|^2 d\mathbb{P} \\ &\leq \int_{\Omega \times \Omega} 2\|\mathbf{X}_0\|^2 + 2\|\mathbf{K}(s)\|^2 + 2\|\mathbf{X}_0\|^2 + 2\|\mathbf{K}(t)\|^2 d\mathbb{P} < \infty, \end{aligned}$$

since  $P_{\mathbf{X}_0} \in \mathcal{P}_2(\mathbb{R}^d)$ , and by using (36) with  $s = 0$  or  $t = 0$ , respectively. Hence,  $\pi$  is an admissible transport plan between  $\mu_s$  and  $\mu_t$ .

Then, we conclude, again using (36), that

$$W_2^2(\mu_s, \mu_t) \leq \int_{\mathbb{R}^d \times \mathbb{R}^d} \|x - y\|^2 d\pi(x, y) = \int_{\Omega \times \Omega} \|\mathbf{X}_s - \mathbf{X}_t\|^2 d\mathbb{P} \leq d c^2 |t - s|^2.$$

Hence,  $(\mu_t)_{t \geq 0}$  is Lipschitz continuous in  $\mathcal{P}_2(\mathbb{R}^d)$  with constant  $d^{\frac{1}{2}}c$ .

ii) By definition (1) and Part i), we see immediately that  $(\mu_t)_{t \geq 0}$  is an absolutely continuous curve. Then it follows from [3, Theorem 8.3.1] that there is a (optimal) velocity field in the continuity equation fulfilling (35).

iii) Let  $\bar{\Omega}_0 := \text{supp}(P_{\mathbf{X}_0})$ . Consider the covering  $\bar{\Omega}_t := \bigcup_{x \in \bar{\Omega}_0} \mathbb{B}_{d^{\frac{1}{2}}ct}(x)$  of  $\bar{\Omega}_0$  with balls of radius  $d^{\frac{1}{2}}ct$ . By (36) it follows that  $\mathbf{X}_t \in \bar{\Omega}_t$   $\mathbb{P}$ -almost surely, yielding the claim  $\text{supp}(P_{\mathbf{X}_t}) \subseteq \bar{\Omega}_t$ .  $\square$

By the next theorem the convergence result from Theorem 8 stated for the insertion method (29) holds also true for our componentwise Kac process (34).

**Theorem 11.** *Let  $f_0$  be a probability density of a random variable  $\mathbf{X}_0 = (X_0^1, \dots, X_0^d)$  with independent components such that  $f_0(x) = f_0(x^1, \dots, x^d) = \prod_{i=1}^d f_0^i(x^i)$  and  $f_0^i \in H^2(\mathbb{R})$ ,  $i = 1, \dots, d$ . Let  $\mathbf{X}(t)$  be a  $d$ -dimensional Kac process starting in  $\mathbf{X}_0$  with parameters  $a > 0$  and  $c \geq c_0 > 0$  and with probability density  $u_t$ . Further, let  $\sigma^2 := \frac{c^2}{a}$  be fixed and  $\mathbf{X}_0 + \sigma \mathbf{W}(t)$  be a  $d$ -dimensional Wiener process starting in  $\mathbf{X}_0$  with probability density  $h_t$ . Assume that  $\mathbf{X}_0$  is independent of  $\mathbf{K}(t)$  and  $\sigma \mathbf{W}(t)$ , respectively. Then it holds*

$$\|h(t, \cdot) - u(t, \cdot)\|_{L_2(\mathbb{R}^d)} \leq C_d \left( \frac{1}{at^{1+\frac{d-1}{4}}} + \frac{1}{ca^{\frac{1}{2}}t^{\frac{1}{2}+\frac{d-1}{4}}} \right) + R_d(a, c, t),$$

where the constant  $C_d$  depends on  $c_0$  and  $\sigma$ , and the function  $R_d(a, c, t)$  satisfies  $\lim_{a, c \uparrow \infty} R_d(a, c, t) = 0$  for any  $t$ , and  $R_d(a, c, \cdot) \in \mathcal{O}(t^{-(\frac{1}{2}+\frac{d}{4})})$  for any  $a, c$ . Hence, the density of our multi-dimensional Kac process  $L_2$ -converges to the density of the Wiener process with rate  $\mathcal{O}(t^{-(\frac{1}{2}+\frac{d-1}{4})})$ .

*Proof.* First, by assumption,  $(X_0^1, \dots, X_0^d, K^1(t), \dots, K^d(t))$  is (mutually) independent. Hence,  $\mathbf{X}_t = (X_0^1 + K^1(t), \dots, X_0^d + K^d(t))$  has independent components  $X_0^i + K^i(t)$  that are one-dimensional Kac processes starting in  $X_0^i \sim f_0^i$ . By Theorem 1, they admit a probability density  $u^i$  solving the 1D telegrapher's equation (30) with initial functions  $f_0^i \in H^2(\mathbb{R})$ , and hence,  $\mathbf{X}_t$  admits the probability density  $u(t, x) = \prod_{i=1}^d u^i(t, x^i)$  by the independence of the components.

Analogously, we conclude that  $\mathbf{X}_0 + \sigma \mathbf{W}(t)$  has the density  $h(t, x) = \prod_{i=1}^d h^i(t, x^i)$ , where the marginal densities  $h^i$  solve the 1D heat equation (32) with initial functions  $f_0^i \in H^2(\mathbb{R})$ . Hence, by Theorem 8, the bound (33) holds componentwise with some  $C_1 = C_1(c_0) > 0$ , i.e.

$$\|h^i(t, \cdot) - u^i(t, \cdot)\|_{L_2(\mathbb{R}^1)} \leq C_1 \left( \frac{1}{at} + \frac{1}{c(ta)^{\frac{1}{2}}} \right) \quad \text{for all } i = 1, \dots, d.$$

Now we show the claim by induction on the dimension  $d$ . The above inequality implies the assertion for  $d = 1$ . Let the claim be true for  $d \geq 1$ . Using that for  $a_i, b_i \in \mathbb{R}$  it holds

$$\prod_{i=1}^{d+1} a_i - \prod_{i=1}^{d+1} b_i = \left( \prod_{i=1}^d a_i \right) (a_{d+1} - b_{d+1}) + b_{d+1} \left( \prod_{i=1}^d a_i - \prod_{i=1}^d b_i \right),$$

it follows by Minkowski's inequality that

$$\begin{aligned}
\|h(t, \cdot) - u(t, \cdot)\|_{L_2(\mathbb{R}^{d+1})} &= \left( \int_{\mathbb{R}^{d+1}} \left| \prod_{i=1}^{d+1} h^i(t, x^i) - \prod_{i=1}^{d+1} u^i(t, x^i) \right|^2 dx \right)^{\frac{1}{2}} \\
&\leq \left( \int_{\mathbb{R}^{d+1}} \left| \left( \prod_{i=1}^d h^i(t, x^i) \right) (h^{d+1}(t, x^{d+1}) - u^{d+1}(t, x^{d+1})) \right|^2 dx \right)^{\frac{1}{2}} \\
&\quad + \left( \int_{\mathbb{R}^{d+1}} |u^{d+1}(t, x^{d+1})| \left( \prod_{i=1}^d h^i(t, x^i) - \prod_{i=1}^d u^i(t, x^i) \right)^2 dx \right)^{\frac{1}{2}} \\
&= \left( \prod_{i=1}^d \|h^i(t, x^i)\|_{L_2(\mathbb{R}^1)} \right) \|h^{d+1}(t, x^{d+1}) - u^{d+1}(t, x^{d+1})\|_{L_2(\mathbb{R}^1)} \\
&\quad + \|u^{d+1}(t, x^{d+1})\|_{L_2(\mathbb{R}^1)} \left( \int_{\mathbb{R}^d} \left| \left( \prod_{i=1}^d h^i(t, x^i) - \prod_{i=1}^d u^i(t, x^i) \right) \right|^2 dx \right)^{\frac{1}{2}}.
\end{aligned}$$

Note that with the one-dimensional heat kernel  $K_\sigma(t, \cdot)$ , Young's inequality for convolutions gives

$$\|h^i(t, \cdot)\|_{L_2} = \|K_\sigma(t, \cdot) * f_0^i\|_{L_2} \leq \|K_\sigma(t, \cdot)\|_{L_2} \|f_0^i\|_{L_1} = \|K_\sigma(t, \cdot)\|_{L_2} = \frac{1}{(4\pi\sigma^2t)^{\frac{1}{4}}}.$$

Hence, the first summand can be estimated by

$$\frac{C_1}{(4\pi\sigma^2)^{\frac{d}{4}}} \left( \frac{1}{at^{1+\frac{d}{4}}} + \frac{1}{ca^{\frac{1}{2}}t^{\frac{1}{2}+\frac{d}{4}}} \right).$$

By the induction hypothesis, the second summand can be estimated by

$$\begin{aligned}
&\left( \|u^{d+1}(t, x^{d+1}) - h^{d+1}(t, x^{d+1})\|_{L_2(\mathbb{R}^1)} + \|h^{d+1}(t, x^{d+1})\|_{L_2(\mathbb{R}^1)} \right) \\
&\quad \cdot \left( C_d \left( \frac{1}{at^{1+\frac{d-1}{4}}} + \frac{1}{ca^{\frac{1}{2}}t^{\frac{1}{2}+\frac{d-1}{4}}} \right) + R_d(a, c, t) \right) \\
&\leq \left( C_1 \left( \frac{1}{at} + \frac{1}{c(ta)^{\frac{1}{2}}} \right) + \frac{1}{(4\pi\sigma^2t)^{\frac{1}{4}}} \right) \\
&\quad \cdot \left( C_d \left( \frac{1}{at^{1+\frac{d-1}{4}}} + \frac{1}{ca^{\frac{1}{2}}t^{\frac{1}{2}+\frac{d-1}{4}}} \right) + R_d(a, c, t) \right).
\end{aligned}$$

Straightforward multiplication finishes the proof.  $\square$

The above assumption on the independence of the initial components  $(X_0^1, \dots, X_0^d)$  was made for simplicity reasons. The convergence result for  $t \rightarrow \infty$  appears to hold true more generally and we forgo the technical details. Furthermore, weak convergence results concerning the paths of a rescaled Kac process towards a Brownian motion can be found in [14, 38].

## 6 Velocity Field of the Multi-Dimensional Kac Flow

In this section, we want to develop a method how to retrieve the velocity field  $v_t$  of the Kac flow in multiple dimensions. By conditioning on single points  $x_0 \in \mathbb{R}^d$ , the multi-dimensional velocity

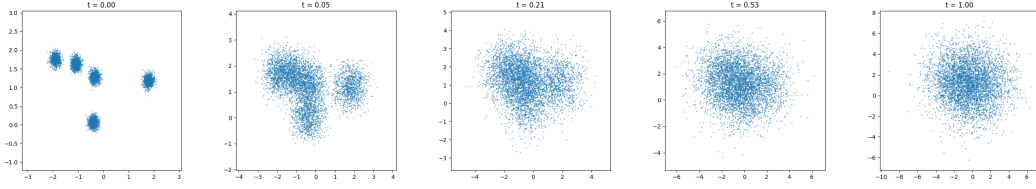


Figure 3: The distribution of  $\mathbf{X}_t$  starting in a 2D Gaussian mixture, simulated until time  $T = 3$  with 'large' parameters  $(a, c) = (100, 10)$ . As described in Theorem 11, we see a 'diffusion' like process with approximate variance  $\sigma^2 t = \frac{c^2}{a} t = t$ .

field  $v_t(x|x_0)$  decomposes into univariate velocities  $v_t^i(x^i|x_0^i)$  which are analytically and numerically accessible. These conditional velocity fields can then be used to approximate the true velocity field  $v_t$  within the framework of conditional flow matching. But note that conceptually, our velocities are conditioned to start at  $t = 0$  in the target measure – reversing the direction of usual flow matching.

The following general lemma states that the velocity field of a multi-dimensional Wasserstein flow can be retrieved by its 1D components if the probability flow admits a multiplicative decomposition (by independence).

**Lemma 12.** *Let  $\mu_t \in AC^2(I; \mathcal{P}_2(\mathbb{R}^d))$  such that*

$$\mu_t(x) = \prod_{i=1}^d \mu_t^i(x^i) \quad \text{for all } x = (x^1, \dots, x^d).$$

Furthermore, assume that the one-dimensional measure flows  $\mu_t^i$  satisfy  $\mu_t^i \in AC^2(I; \mathcal{P}_2(\mathbb{R}))$  and a continuity equation with some vector field  $v_t^i$ , i.e.

$$\partial_t \mu_t^i(x^i) = -\partial_{x^i}(\mu_t^i(x^i)v_t^i(x^i)) \quad \text{for all } x^i \in \mathbb{R}.$$

Then  $\mu_t$  satisfies the continuity equation  $\partial_t \mu_t(x) = -\nabla \cdot (\mu_t(x)v_t(x))$  with the velocity field

$$v_t(x) := (v_t^1(x^1), \dots, v_t^d(x^d)) \quad \text{for all } x = (x^1, \dots, x^d).$$

*Proof.* First, we give a formal derivation of the result, and justify the calculations more rigorously afterwards. We compute  $\partial_t \mu_t(x)$  formally by use of the product rule and obtain

$$\partial_t \mu_t(x) = \sum_{i=1}^d \left( \prod_{j \neq i}^d \mu_t^j(x^j) \right) \partial_t \mu_t^i(x^i).$$

Using the continuity equation for  $\mu_t^i$ , we obtain

$$\partial_t \mu_t(x) = -\sum_{i=1}^d \left( \prod_{j \neq i}^d \mu_t^j(x^j) \right) \partial_{x^i}(\mu_t^i(x^i)v_t^i(x^i)).$$

Pulling the product which does not depend on  $x^i$  into the  $\partial_{x^i}$ -derivative, formally yields the claim

$$\partial_t \mu_t(x) = -\sum_{i=1}^d \partial_{x^i}(\mu_t(x)v_t^i(x^i)) = -\nabla \cdot (\mu_t(x)v_t(x)).$$

More precisely, we can test above equations by product test functions  $\phi(t, x) = \prod_{i=1}^d \phi^i(t, x^i)$  with  $\phi^i \in C_c^\infty((0, \infty) \times \mathbb{R})$ , and obtain the result in the weak formulation. Finally, since the linear subspace generated by such products is dense in  $C_c^\infty((0, \infty) \times \mathbb{R}^d)$  and by Lebesgue's dominated convergence, this yields the claim.  $\square$

The following main theorem will be of fundamental importance for the generative modeling via the Kac flow. In particular, we obtain an analytical formula for the conditional velocity field  $v_t(x|x_0)$  of a Kac process conditioned to start in a point  $x_0 \in \mathbb{R}^d$ .

**Theorem 13.** *For a fixed  $x_0 \in \mathbb{R}^d$ , let  $\mathbf{X}_t := x_0 + \mathbf{K}(t)$  be the Kac process starting in  $x_0$ . Then,  $\mu_t(\cdot|x_0) := P_{\mathbf{X}_t}$  satisfies a continuity equation (2) with the velocity field*

$$v_t(x|x_0) := (v_t^1(x^1|x_0^1), \dots, v_t^d(x^d|x_0^d)) \quad \text{for all } x = (x^1, \dots, x^d), \quad (37)$$

where the univariate components  $v_t^i(x^i|x_0^i)$  are given by

$$v_t^i(x^i|x_0^i) := \begin{cases} (x^i - x_0^i) \left( t + \frac{r_t(x^i - x_0^i)}{c} \cdot \frac{I_0(\beta r_t(x^i - x_0^i))}{I_0'(\beta r_t(x^i - x_0^i))} \right)^{-1} & \text{if } x^i \in (x_0^i - ct, x_0^i + ct), \\ c & \text{if } x^i = x_0^i + ct, \\ -c & \text{if } x^i = x_0^i - ct, \\ \text{arbitrary} & \text{otherwise.} \end{cases} \quad (38)$$

Furthermore, it holds

$$v_t^i(x^i|x_0^i) = \mathbb{E}[\dot{X}^i(t) \mid X_t^i = x^i, X_0^i = x_0^i]. \quad (39)$$

*Proof.* By Proposition 10,  $\mu_t(\cdot|x_0)$  admits a velocity field  $v_t(\cdot|x_0)$  satisfying the continuity equation (2). By construction, the components  $(X_t^1, \dots, X_t^d)$  of  $\mathbf{X}_t$  are mutually independent. Hence,  $\mu_t(x|x_0) = \prod_{i=1}^d \mu_t^i(x^i|x_0^i)$ , where the one-dimensional probability flows  $\mu_t^i(\cdot|x_0^i)$  fulfill a continuity equation with 1D velocity fields  $v_t^i(\cdot|x_0^i)$ . By Lemma 12, it holds the decomposition (37), and Theorem 4 immediately gives the formula (38). Finally, [21, Theorem 3.3], resp. [43, Theorem 6.3] provides (39).  $\square$

In stochastic analysis, the relation (39) has been known in connection with the *mimicking of stochastic processes*, see e.g. [5, 13]. Here, the mimicking process is given by the flow ODE (5).

Having identified the conditional vector field  $v_t(\cdot|x_0)$  for the conditional distribution  $\mu_t(\cdot|x_0)$  of the Kac process, we get the following result by employing [19], see also [43, Theorem 5.1, Remark 5.3], with slight adjustments to our setting.

**Corollary 14.** *Let  $\mathbf{X}_t$  be the multi-dimensional Kac process starting in  $\mathbf{X}_0 \sim \mu_0 \in \mathcal{P}_2(\mathbb{R}^d)$ . Assume that  $\mathbf{X}_0$  is independent of  $\mathbf{K}(t)$ , and assume that  $\mathbf{X}_0$  has a density  $f_0$ . Then, the marginal distribution of  $\mathbf{X}_t$  admits the density  $u_t$  given by*

$$u_t(x) = \int u_t(x|x_0) f_0(x_0) dx_0,$$

where  $u_t(\cdot|x_0)$  is the conditional distribution of  $\mathbf{X}_t$  conditioned to  $\mathbf{X}_0 = x_0$ , and by symmetry<sup>3</sup>,  $u_t(x|\cdot)$  is exactly the distribution  $u_t(\cdot|x)$  for any  $x \in \mathbb{R}^d$ .

<sup>3</sup>This is *not* an application of Bayes' rule.

Denote the conditional velocity field corresponding to  $u_t(\cdot|x_0)$  by  $v_t(\cdot|x_0)$ . By independence of  $\mathbf{X}_0$  and  $\mathbf{K}(t)$ , it is given via (38), and finally, the vector field

$$v_t(x) := \frac{1}{u_t(x)} \int u_t(x|x_0) v_t(x|x_0) f_0(x_0) dx_0$$

satisfies the continuity equation

$$\partial_t u_t(x) = -\nabla \cdot (u_t(x)v_t(x))$$

in the distributional sense.

Now we have all the ingredients to define a feasible loss function for learning the above velocity field  $v_t$  by a neural network  $v_t^\theta$ . Clearly, it is desirable to use the loss

$$\mathcal{L}(\theta) := \mathbb{E}_{(t,x) \sim \mathcal{U}(0,T) \times_t u_t} \left[ \|v^\theta(t,x) - v(t,x)\|^2 \right],$$

where  $\mathcal{U}(0,T) \times_t u_t$  is understood in the sense of *disintegration*, see [43, Ch. 2.3], but here we have no direct access to  $v$ . However, following the same lines as in [19], we see that

$$\mathcal{L}(\theta) = \mathcal{L}_{\text{CFM}}(\theta) + \text{const}$$

with a constant not depending on  $\theta$ , and the Conditional Flow Matching (CFM) loss is given by

$$\mathcal{L}_{\text{CFM}}(\theta) = \mathbb{E}_{t \sim \mathcal{U}(0,T), x_0 \sim \mu_0, x \sim u_t(\cdot|x_0)} \left[ \|v^\theta(t,x) - v(t,x|x_0)\|^2 \right]. \quad (40)$$

Here, we have access to both  $v(t,x|x_0)$  and  $u_t(\cdot|x_0)$  via (37) and (19), respectively, which we will exploit in the next section.

**Remark 15.** Notice that the decomposition of velocity fields from Lemma 12 holds generally and independently from our specific Kac model. Hence, our approach of decomposing the conditional velocity in conjunction with conditional flow matching is generally applicable to any model with a componentwise forward process (i.e. independent components).

## 7 Numerical Experiments

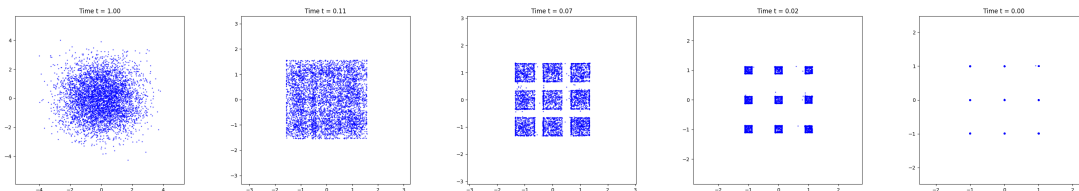


Figure 4: Backward evolution of the *learned* Kac flow for  $(a, c) = (25, 5)$ , see also Figure 5.

In this section, we use the flow matching framework to train a neural network to approximate the velocity field from Corollary 14 by minimizing the CFM loss given in (40). To this end, we

compute the conditional velocity  $v_t(x|x_0)$  via its analytic formula (38). In order to sample from  $\mathbf{X}_t \sim u_t(\cdot|x_0)$ , where  $x_0$  is fixed, we only need to sample i.i.d. components  $X_t^i$  of the Kac process starting in 0. This can be done efficiently, since we have access to the analytic form (19) of the one-dimensional Kac distribution starting in 0 (use e.g. inverse transform sampling). Further, if we wish to sample fixed realizations of a Kac process for varying times  $t$ , we can efficiently simulate the random walk itself as explained in Appendix A.1.

During inference, we sample the latent variable from the Kac process  $K_T$  starting in zero, at a final time  $T$ , and then integrate the flow ODE (5) backwards in time using an ODE solver with the learned vector field as the drift. Using the standard Kac flow introduces an approximation error, namely the distance between  $X_T$  and  $K_T$ . This can be avoided by applying the mean reverting Kac flow (41) which we will introduce below.

## 7.1 Diffusion vs. Kac Process: A 2D Experiment with Dirac-like Modes

In (8), we verified that velocity fields of diffusion flows admit a local explosion at small times  $t \approx 0$ , when starting in Dirac points. In contrast, the multi-dimensional Kac flow enjoys a globally bounded velocity field as proven in Proposition 10. We want to demonstrate this difference in the qualitative behavior by the following toy problem in 2D: as ground truth we choose an equally weighted Gaussian mixture with 9 modes on a  $3 \times 3$  grid, where each mode is given by an isotropic Gaussian with *small* standard deviation  $\sigma = 0.0001$ , representing some Dirac points, see Figure 5. We apply the conditional flow matching framework to both the Kac and diffusion based model. Here we use the Kac process (16) starting in the data with parameters  $\frac{c^2}{a} = 1$ , and the standard diffusion with parameter  $\sigma = 1$  and the velocity field (7).

We trained each model for 500k iterations, and used the negative log-likelihood as a validation loss. In Figure 5 we plot the resulting generated samples and report the associated training iterations. The complete experimental setup can be found in the Appendix A.2. For the backward evolution of the learned (25, 5)-Kac flow, see Figure 4.

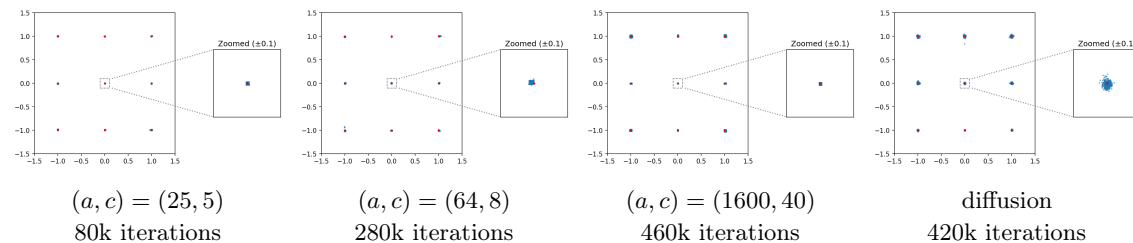


Figure 5: Generated samples (blue) vs. ground truth (red) at the indicated iteration for each model. The Kac model can precisely recover the small modes, while the diffusion model creates "blobs".

In contrast to our Kac generative model, the diffusion based model is not able to precisely approximate the Dirac-like modes, even with long training times and vanishing truncation times<sup>4</sup>  $\epsilon \approx 0$ . Clearly, high choices of parameters  $(a, c)$  lead to diffusion-like results as theoretically underlined in Theorem 11.

<sup>4</sup>By the explosion (8) time truncations were necessary, since otherwise the associated adaptive step size ODE solver diverged with intended step size going to 0.

## 7.2 Image Generation

In general, the 'standard' Kac process  $X_t = X_0 + K_t$  and  $K_t$  themselves are not equal at the final time  $T$ . It is common practice in generative modeling to augment the process so that the data no longer contributes to the final distribution (compare with variance-preserving diffusion processes, e.g. the Ornstein–Uhlenbeck process). Additionally, we introduce a time-scheduling function for the noising process. Let  $X_0$  and  $K(t)$  be independent, and for simplicity, we fix  $T = 1$  for the rest of this section.

**The Mean-Reverting Kac Process.** We define the *mean-reverting* Kac process by

$$M_t := f(t) X_0 + K_{g(t)}, \quad t \in [0, 1], \quad (41)$$

for smooth functions  $f, g$  satisfying

$$f(0) = 1, \quad f(1) = 0 \quad \text{and} \quad g(0) = 0, \quad g(1) = 1.$$

In particular,  $M_1 = K_1$ . Differentiating (41) gives

$$\dot{M}_t = \dot{f}(t) X_0 + \dot{g}(t) \dot{K}_{g(t)},$$

and hence the conditional velocity field is given by

$$\begin{aligned} v_M(t, x \mid x_0) &= \mathbb{E}[\dot{M}_t \mid M_t = x, X_0 = x_0] \\ &= \mathbb{E}[\dot{f}(t) x_0 + \dot{g}(t) \dot{K}_{g(t)} \mid K_{g(t)} = x - f(t)x_0, X_0 = x_0] \\ &= \dot{f}(t) x_0 + \dot{g}(t) v_K(g(t), x - f(t)x_0 \mid 0), \end{aligned} \quad (42)$$

where  $v_K(t, x \mid 0)$  is the conditional Kac velocity field from (37). Note that in the last equality, the independence of  $X_0$  and  $K(t)$  is used to drop the condition  $X_0 = x_0$ . Now, by the same arguments as in Corollary 14, one recovers the corresponding vector field for the mean-reverting Kac process.

**Connection to Flow Matching.** Now let  $R_t := f(t)X_0 + B_{g(t)}$  with a standard Brownian motion  $B_t$ . If we choose

$$f(t) = 1 - t, \quad g(t) = t^2,$$

then it holds

$$R_t = (1 - t) X_0 + B_{t^2} \stackrel{d}{=} (1 - t) X_0 + t B_1, \quad t \in [0, 1]. \quad (43)$$

Notice that (43) matches exactly the forward process used in recent flow matching works, see [19, 43]. We experimented with various schedules and found that the above flow matching pair

$$(f, g) = (1 - t, t^2)$$

also yielded good generation results for our Kac model. In the following, we compare our approach via  $(M_t)_t$  with that using the process  $(R_t)_t$ , in particular with flow matching based on the independent coupling.

**CIFAR-10.** We test our approach on generating CIFAR-10 images. We train the velocity field using conditional flow matching with the vector field (42) and compare a variety of choices for  $(a, c)$  and the schedules  $g(t) = t$  and  $g(t) = t^2$ . We apply a UNET architecture to parameterize the velocity field and use an ODE solver to simulate the corresponding flow ODE. We aligned our hyperparameters with those employed in [41] to train our models. Our code is available online<sup>1</sup>. For further details we refer to the implementation details in Appendix A.2.

In Table 7.2 we report the FID results of our Kac methods via  $M_t$  as well as the diffusion baselines via  $R_t$ . We implemented the baseline models ourselves and denote them by "Diff" for  $g(t) = t$  and "FM" for  $g(t) = t^2$ . In Figures 6, 7 we plot a selection of the generated images. Recall that the parameter  $a$  corresponds to the damping coefficient and  $c$  to the propagation speed. The schedule  $g(t) = t$  generally led to worse performance, especially for the baseline and our methods with diffusion-like parameters. However certain combinations of high damping and low velocity pairs  $(a, c)$  such as  $(25, 2)$  were able to perform well. In contrast the schedule  $g(t) = t^2$  improved the baseline substantially, and our methods across the board. With this experiment we aim to demonstrate the scalability of our method, an extensive study of the effect of the parameters  $(a, c)$  is not in the scope of the paper and left to future work. For further visual examples see Appendix A.3.

Schedule: $g(t) = t^2$				Schedule: $g(t) = t$			
Method	FID	Method	FID	Method	FID	Method	FID
$a = 900, c = 10$	<b>7.26</b>	$a = 100, c = 10$	10.01	$a = 900, c = 10$	17.63	$a = 100, c = 10$	39.93
$a = 900, c = 20$	7.46	$a = 25, c = 1$	8.60	$a = 900, c = 20$	42.46	$a = 25, c = 1$	8.31
$a = 900, c = 30$	8.05	$a = 25, c = 2$	8.65	$a = 900, c = 30$	64.60	$a = 25, c = 2$	<b>6.42</b>
$a = 100, c = 1$	11.41	$a = 25, c = 3$	9.15	$a = 100, c = 1$	11.64	$a = 25, c = 3$	7.95
$a = 100, c = 3$	7.77	$a = 25, c = 4$	9.56	$a = 100, c = 3$	8.56	$a = 25, c = 4$	10.59
$a = 100, c = 5$	7.73	$a = 25, c = 5$	10.70	$a = 100, c = 5$	14.66	$a = 25, c = 5$	16.81
$a = 100, c = 7$	8.58	FM (our impl.)	7.59	$a = 100, c = 7$	24.44	Diff (our impl.)	82.27

Table 1: FID (100-step Euler) for  $(a, c)$ -Kac under two time schedules.

**Acknowledgement.** J. Chemseddine acknowledges funding of the DFG project STE 571/17-2 within the SPP 2298 "Theoretical Foundations of Deep Learning". R. Duong, P. Friz and G. Steidl acknowledge funding of the project EF-LI-Opt-2 within the DFG Excellence Cluster MATH+. The work of P. Friz is also supported by DFG CRC/TRR 388, project A02. Our thanks go to Gregor Kornhardt, Matthias Liero, Nicolaj Rux, and Weiqiao Han for fruitful discussions. We are especially grateful to Weiqiao Han for correcting an error in our implementation.

## References

- [1] M. S. Albergo, N. M. Boffi, and E. Vanden-Eijnden. Stochastic interpolants: A unifying framework for flows and diffusions. *arXiv preprint arXiv:2303.08797*, 2023.
- [2] M. S. Albergo and E. Vanden-Eijnden. Building normalizing flows with stochastic interpolants. *ICLR*, 2022.

<sup>1</sup><https://github.com/JChemseddine/telegraphers>



Figure 6: Generation results of the best performing mean-reverting Kac models and the diffusion baseline (flow matching) for  $g(t) = t^2$ .

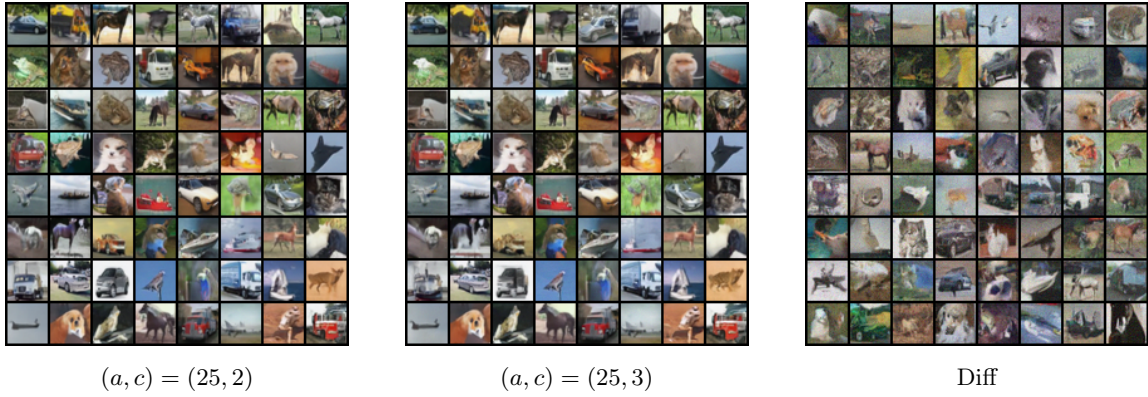


Figure 7: Generation results of the best performing mean-reverting Kac models and the diffusion baseline for  $g(t) = t$ .

- [3] L. Ambrosio, N. Gigli, and G. Savaré. *Gradient Flows*. Lectures in Mathematics ETH Zürich. Birkhäuser, Basel, 2nd edition, 2008.
- [4] D. Blessing, J. Berner, L. Richter, and G. Neumann. Underdamped diffusion bridges with applications to sampling. *ICLR*, 2025.
- [5] G. Brunick and S. Shreve. Mimicking an Itô process by a solution of a stochastic differential equation. *The Annals of Applied Probability*, 23(4):1584–1628, 2013.
- [6] C. Cattaneo. Sur une forme de l’équation de la chaleur éliminant le paradoxe d’une propagation instantanée. *Comptes Rendus.*, 247:431–433, 1958.
- [7] J. Chemseddine, C. Wald, R. Duong, and G. Steidl. Neural sampling from Boltzmann densities: Fisher-Rao curves in the Wasserstein geometry. *ICLR*, 2025.
- [8] R. T. Q. Chen. torchdiffeq, 2018.

- [9] M. Chester. Second sound in solids. *Physical Review*, 131:2013–2015, 1963.
- [10] T. Dockhorn, A. Vahdat, and K. Kreis. Score-based generative modeling with critically-damped Langevin diffusion. *ICLR*, 2022.
- [11] R. Griego and R. Hersh. Theory of random evolutions with applications to partial differential equations. *Transactions of the American Mathematical Society*, 156:405–418, 1971.
- [12] W. Guo, M. Tao, and Y. Chen. Complexity analysis of normalizing constant estimation: from Jarzynski equality to annealed importance sampling and beyond. *ArXiv:2502.04575*, 2025.
- [13] I. Gyöngy. Mimicking the one-dimensional marginal distributions of processes having an Itô differential. *Probability Theory and Related Fields*, 71:501–516, 1986.
- [14] J. Hui, X. Lihu, and Y. Qingshan. Functional large deviations for Kac–Stroock approximation to a class of Gaussian processes with application to small noise diffusions. *Journal of Theoretical Probability*, 37(4):3015–3054, 2024.
- [15] A. Janssen. The distance between the Kac process and the Wiener process with applications to generalized telegraph equations. *Journal of Theoretical Probability*, 3(2):349–360, 1990.
- [16] Y. M. Kabanov. On the probabilistic representation of a solution of the telegraph equation. *Theory of Probability and its Applications*, 37:379–380, 1993.
- [17] M. Kac. A stochastic model related to the telegrapher’s equation. *Rocky Mountain Journal of Mathematics*, 4(3):497–509, 1974.
- [18] D. Kim, S. Shin, K. Song, W. Kang, and I.-C. Moon. Soft truncation: A universal training technique of score-based diffusion model for high precision score estimation. *ICML*, 2022.
- [19] Y. Lipman, R. Chen, H. Ben-Hamu, M. Nickel, and M. Le. Flow matching for generative modeling. *ICLR*, 2023.
- [20] Q. Liu. Rectified flow: A marginal preserving approach to optimal transport. *arXiv preprint arXiv:2209.14577*, 2022.
- [21] X. Liu, C. Gong, and Q. Liu. Flow straight and fast: Learning to generate and transfer data with rectified flow. *ICLR*, 2023.
- [22] Z. Liu, D. Luo, Y. Xu, T. Jaakkola, and M. Tegmark. GenPhys: from physical processes to generative models. *ArXiv:2304.02637*, 2023.
- [23] D. Lutz. Which operators generate cosine operator functions? *Atti della Accademia Nazionale dei Lincei. Classe di Scienze Fisiche, Matematiche e Naturali. Rendiconti, Serie 8*, 63(5):314–317, 1977.
- [24] S. Martin, A. Gagneaux, P. Hagemann, and G. Steidl. PnP-Flow: Plug-and-play image restoration with flow matching. *ICLR*, 2025.
- [25] J. Masoliver and G. H. Weiss. Finite-velocity diffusion. *European Journal of Physics*, 17:190–196, 1996.

- [26] A. Maurais and Y. Marzouk. Sampling in unit time with kernel Fisher-Rao flow. *ICML*, 2024.
- [27] B. Máté and F. Fleuret. Learning interpolations between Boltzmann densities. *Transactions on Machine Learning Research*, 2023.
- [28] A. Q. Nichol and P. Dhariwal. Improved denoising diffusion probabilistic models. In *International conference on machine learning*, pages 8162–8171. PMLR, 2021.
- [29] M. Nualart. Distributional solutions for damped wave equations. *Electronic Journal of Differential Equations*, 2020(131):1–16, 2020.
- [30] N. Nüsken. Stein transport for Bayesian inference. *arXiv preprint arXiv:2409.01464*, 2024.
- [31] A. Obukhov, M. Seitzer, P.-W. Wu, S. Zhydenko, J. Kyl, and E. Y.-J. Lin. High-fidelity performance metrics for generative models in pytorch, 2020.
- [32] H. G. Othmer and T. Hillen. The diffusion limit of transport equations derived from velocity-jump processes. *SIAM Journal on Applied Mathematics*, 61(3):751–775, 2000.
- [33] J. Pidstrigach. Score-based generative models detect manifolds. *NeurIPS*, 2022.
- [34] G. Plonka, D. Potts, G. Steidl, and M. Tasche. *Numerical Fourier Analysis*. Birkhäuser, Basel, 2nd edition, 2023.
- [35] J. Sohl-Dickstein, E. Weiss, N. Maheswaranathan, and S. Ganguli. Deep unsupervised learning using nonequilibrium thermodynamics. In F. Bach and D. Blei, editors, *Proceedings of the 32nd International Conference on Machine Learning*, volume 37 of *Proceedings of Machine Learning Research*, pages 2256–2265, Lille, France, 07–09 Jul 2015. PMLR.
- [36] Y. Song and S. Ermon. Generative modeling by estimating gradients of the data distribution. *NeurIPS*, 2019.
- [37] Y. Song, J. Sohl-Dickstein, D. P. Kingma, A. Kumar, S. Ermon, and B. Poole. Score-based generative modeling through stochastic differential equations. *ICLR*, 2021.
- [38] D. Stroock. *Lectures on Topics in Stochastic Differential Equations*. Tata Institute of Fundamental Research & Springer, 1982.
- [39] J. Sun, J. Berner, L. Richter, M. Zeinhofer, J. Müller, K. Azizzadenesheli, and A. Anandkumar. Dynamical measure transport and neural PDE solvers for sampling. *arXiv:2407.07873*, 2024.
- [40] R. C. Tautz and I. Lerche. Application of the three-dimensional telegraph equation to cosmic-ray transport. *Research in Astronomy and Astrophysics*, 16(10):162–170, 2016.
- [41] A. Tong, K. Fatras, N. Malkin, G. Huguet, Y. Zhang, J. Rector-Brooks, G. Wolf, and Y. Bengio. Improving and generalizing flow-based generative models with minibatch optimal transport. *Transactions on Machine Learning Research*, pages 1–34, 2024.
- [42] P. Vernotte. Les paradoxes de la theorie continue de l’équation de la chaleur. *Comptes Rendus.*, 246:3154–3155, 1958.

- [43] C. Wald and G. Steidl. Flow Matching: Markov kernels, stochastic processes and transport plans. In *Variational and Information Flows in Machine Learning and Optimal Transport, Oberwolfach Seminars. Vol. 56*, pages 185–254. Birkhäuser, 2025.
- [44] Y. Xu, Z. Liu, M. Tegmark, and T. Jaakkola. Poisson flow generative models. *NeurIPS*, 2022.
- [45] B. Zhang, W. Yu, and M. Mascagni. Revisiting Kac’s method: A Monte Carlo algorithm for solving the telegrapher’s equations. *Mathematics and Computers in Simulation*, 156:176–198, 2018.
- [46] Y. Zhu, K. Zhang, J. Liang, J. Cao, B. Wen, R. Timofte, and L. Van Gool. Denoising diffusion models for plug-and-play image restoration. In *IEEE/CVF Conference on Computer Vision and Pattern Recognition (CVPR) Workshop*, pages 1219–1229, 2023.

## A Appendix: Additional Material

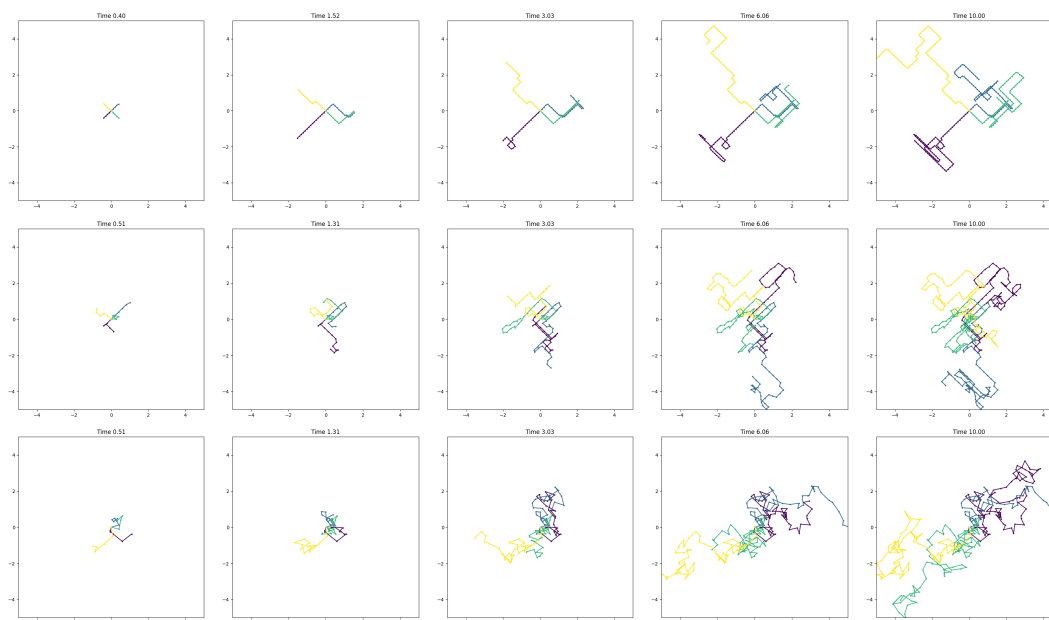


Figure 8: Paths of the componentwise Kac walk in 2D, simulated until time  $T = 10$  with  $(a, c) = (1, 1)$  (upper row),  $(a, c) = (4, 2)$  (middle row) and  $(a, c) = (25, 5)$  (lower row).

### A.1 Simulating the Kac Process

Recall that the Kac process  $K_t$  starting in 0 is given by

$$K(t) := B_{\frac{1}{2}} c \tau_t,$$

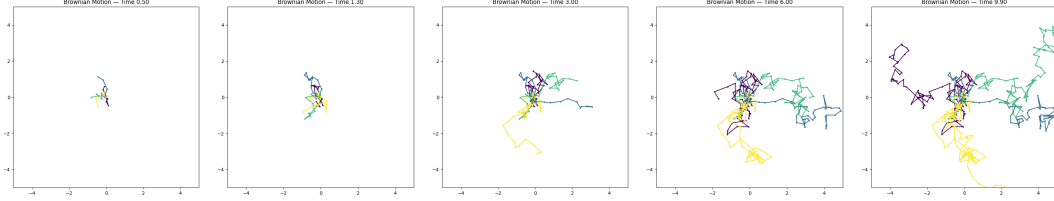


Figure 9: Paths of a standard Brownian motion in 2D, simulated until time  $T = 10$ .

therefore we need to sample from the random times  $\tau_t$ . Since the process is i.i.d. we outline the procedure for the one-dimensional case, in higher dimensions the same procedure is done component-wise.

We follow the approach proposed in [45]. Let  $N(t)$  be a Poisson process with rate  $a > 0$ , recall that  $\tau_t = \int_0^t (-1)^{N(s)} ds$ . Suppose that the times at which the Poisson process jumps are given by  $0 < j_1 < j_2 < \dots < j_{N(t)} < t$ . Then  $\tau_t$  can be expressed exactly as

$$\tau_t = j_1 + \sum_{k=1}^{N(t)-1} (-1)^k (j_{k+1} - j_k) + (-1)^{N(t)} (t - j_{N(t)}).$$

where we define  $j_0 := 0$ .

It is well known that the waiting times between jumps  $s_k := (j_{k+1} - j_k)$  are exponentially distributed with parameter  $a$ . We can therefore sample  $s_k$  and compute the corresponding sum by determining the instance when their cumulative sum exceeds  $t$ .

To evaluate this quantity efficiently, we begin by sampling a fixed number of i.i.d. exponential random variables  $s_k \sim \text{Exp}(a)$  for  $k = 1, \dots, \kappa$ , where  $\kappa$  is a sufficiently large upper bound. We then compute the cumulative sums  $S_k = \sum_{j=1}^k s_j$ .

Given a target time  $t$ , we identify the smallest index  $n$  such that  $S_n > t$ , and compute

$$\tau_t = \sum_{k=1}^{n-1} (-1)^{k-1} s_k + (-1)^{n-1} (t - S_{n-1}).$$

In practice, we set  $\kappa := \lceil 2aT \rceil + b$ , where  $T$  is the maximum time of interest and  $b$  is a small buffer constant (e.g., 20) to ensure sufficient coverage with high probability.

This procedure can be applied independently for multiple values of  $t$ , allowing efficient simulation of the Kac process, see Algorithm A.1.

## A.2 Implementation Details

For all experiments we sampled from the Kac process using the following algorithm A.2. We outline the sampling procedure for the 1D Kac density, for the multidimensional process we use this procedure component-wise.

**2D Toy Experiment.** As the target distribution we use a 9-component Gaussian mixture model (GMM) in  $\mathbb{R}^2$ . Let

$$\{\mu_i\}_{i=1}^9 = \left\{ (u_1, u_2) \mid u_j \in \{-1, 0, 1\} \right\},$$

---

**Algorithm 1** Simulating the Kac process  $\tau_t$ 

---

- 1: **Input:** Time  $t > 0$ , rate  $a > 0$ , upper bound  $T$ , buffer  $b$
  - 2: Set  $\kappa \leftarrow \lceil 2aT \rceil + b$
  - 3: Sample  $s_1, \dots, s_\kappa \sim \text{Exp}(a)$
  - 4: Compute cumulative sums:  $S_k = \sum_{j=1}^k s_j$  for  $k = 1, \dots, \kappa$
  - 5: Find the smallest index  $n$  such that  $S_n > t$
  - 6: Initialize  $\tau \leftarrow 0$
  - 7: **for**  $k = 1$  to  $n - 1$  **do**
  - 8:    $\tau \leftarrow \tau + (-1)^{k-1} s_k$
  - 9: **end for**
  - 10:  $\tau \leftarrow \tau + (-1)^{n-1} (t - S_{n-1})$
  - 11: **Output:**  $\tau_t = \tau$
- 

---

**Algorithm 2** Sampling the 1D Kac density via inverse-CDF

---

- 1: Draw  $U \sim \mathcal{U}(0, 1)$ .
  - 2: **if**  $U < e^{-at}$  **then**
  - 3:   Draw  $\sigma \in \{\pm 1\}$  with  $\Pr(\sigma = \pm 1) = \frac{1}{2}$ .
  - 4:   **Output**  $\sigma c t$  from the atomic terms in (18).
  - 5: **else**
  - 6:   Draw  $V \sim \mathcal{U}(0, 1)$ .
  - 7:   Compute  $x \approx F_{\text{cont}}^{-1}(V; t)$ , where  $F_{\text{cont}}$  is the continuous-part CDF in (19), numerically approximated via a precomputed inverse-CDF table.
  - 8:   Draw  $\sigma \in \{\pm 1\}$  with  $\Pr(\sigma = \pm 1) = \frac{1}{2}$ .
  - 9:   **Output**  $\sigma x$ .
  - 10: **end if**
- 

we use uniform weights and a very small, shared isotropic covariance:

$$w_i = \frac{1}{K}, \quad \Sigma_i = \sigma^2 I_d, \quad \sigma = 10^{-4},$$

and define the mixture density

$$p(x) = \sum_{i=1}^K w_i \mathcal{N}(x; \mu_i, \Sigma_i)$$

We set  $T = 1$  for all models. During inference we use the exact latent

$$X_t := X_0 + K_t,$$

i.e. we draw  $X_0$  directly from our GMM and add the exact Kac noise  $K_t$ , thereby avoiding any sampling approximation in this toy example. Analogously, in the diffusion case, we use a standard Brownian motion  $B_t$  instead of  $K_t$ . All models were trained for 500,000 iterations with a learning rate of  $5 \times 10^{-4}$  and a batch size of 256. For validation we compute the negative log-likelihood (NLL) of  $N$  model-generated samples under the true GMM density:

$$\text{NLL} = -\frac{1}{N} \sum_{n=1}^N \log p(x^{(n)}),$$

where  $x^{(n)}$  are drawn from the learned model. We set  $N = 5000$ . For the velocity field we used a fully-connected MLP with three hidden layers of width  $w = 256$  and ReLU activations. Specifically for the diffusion model we required time truncation, namely we train the flow on the interval  $[\varepsilon, T]$  with  $\varepsilon = 10^{-15}$ . We used the torchdiffeq [8] package to simulate the ODEs with "dopri5" adaptive step size solver.

**CIFAR Experiment.** We trained all models for 400k iterations, a batch size of 128 and a constant learning rate of  $2 \times 10^{-4}$ . We used the torchdiffeq [8] package to simulate the ODEs with an explicit Euler scheme. We use the time dependent U-Net architecture from [28]. We use the same network parameters as in [41], also employing an EMA with decay rate 0.9999. We do not use any data augmentation for training. Note that in our implementation of the diffusion model with schedule  $g(t) = t$ , we use the common time truncation of training on the interval  $[\varepsilon, 1]$  with  $\varepsilon = 10^{-5}$  (see [37]). Both training and evaluation was done using fixed random seeds. The FID is computed on 50k samples using the torch fidelity package [31]. The code is available at <https://github.com/JChemseddine/telegraphers>.

### A.3 Further numerical examples

Here we showcase the CIFAR-10 images generated by our Kac model for other damping/velocity pairs  $(a, c)$ . The corresponding FID scores can be found in Table 7.2.

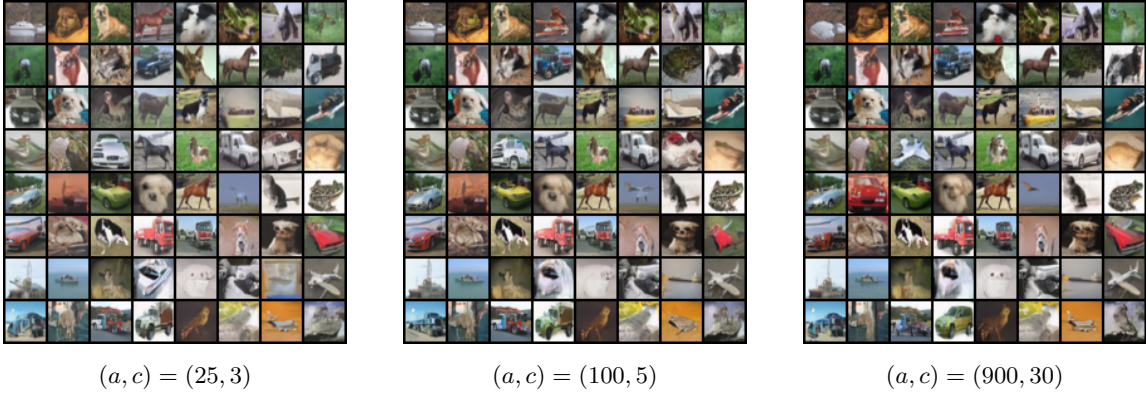


Figure 10: Further generation results of the mean-reverting Kac models with  $g(t) = t^2$ .

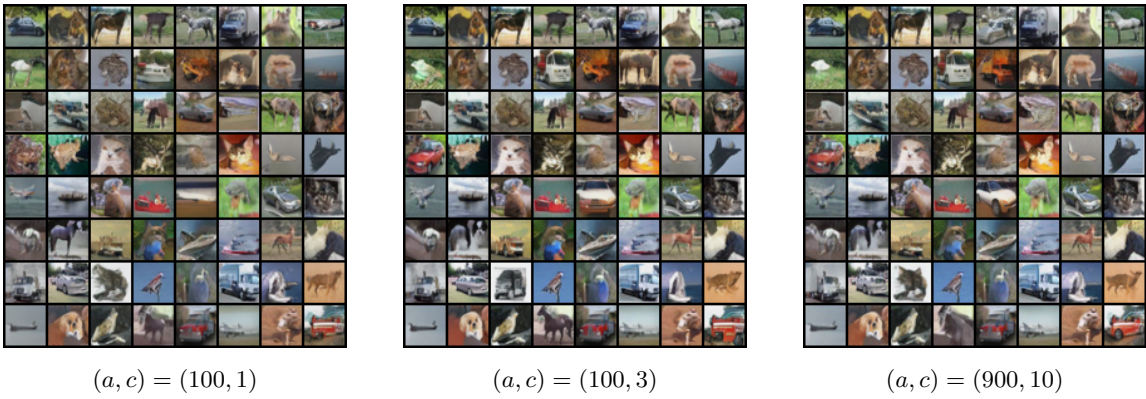


Figure 11: Further generation results of the mean-reverting Kac models with  $g(t) = t$ .